eNeuro

Research Article: New Research
Cognition and Behavior

Reconstructing Spatiotemporal Trajectories of Visual Object Memories in the Human Brain

Julia Lifanov-Carr,[1] Benjamin J. Griffiths,[1] Juan Linde-Domingo,[1,2,3] Catarina S. Ferreira,[1] Martin Wilson,[1] Stephen D. Mayhew,[4] Ian Charest,[5] and Maria Wimber[1,6]

[1]School of Psychology and Centre for Human Brain Health (CHBH), University of Birmingham, Birmingham B15 2TT, United Kingdom, [2]Department of Experimental Psychology, Mind, Brain and Behavior Research Center (CIMCYC), University of Granada, 18011 Granada, Spain, [3]Center for Adaptive Rationality, Max Planck Institute for Human Development, 14195 Berlin, Germany, [4]Institute of Health and Neurodevelopment (IHN), School of Psychology, Aston University, Birmingham B4 7ET, United Kingdom, [5]Département de Psychologie, Université de Montréal, Montréal, Quebec H2V 2S9, Canada, and [6]School of Psychology & Neuroscience and Centre for Cognitive Neuroimaging (CCNi), University of Glasgow, Glasgow G12 8QB, United Kingdom

Abstract

How the human brain reconstructs, step-by-step, the core elements of past experiences is still unclear. Here, we map the spatiotemporal trajectories along which visual object memories are reconstructed during associative recall. Specifically, we inquire whether retrieval reinstates feature representations in a copy-like but reversed direction with respect to the initial perceptual experience, or alternatively, this reconstruction involves format transformations and regions beyond initial perception. Participants from two cohorts studied new associations between verbs and randomly paired object images, and subsequently recalled the objects when presented with the corresponding verb cue. We first analyze multivariate fMRI patterns to map where in the brain high- and low-level object features can be decoded during perception and retrieval, showing that retrieval is dominated by conceptual features, represented in comparatively late visual and parietal areas. A separately acquired EEG dataset is then used to track the temporal evolution of the reactivated patterns using similarity-based EEG–fMRI fusion. This fusion suggests that memory reconstruction proceeds from anterior frontotemporal to posterior occipital and parietal regions, in line with a conceptual-to-perceptual gradient but only partly following the same trajectories as during perception. Specifically, a linear regression statistically confirms that the sequential activation of ventral visual stream regions is reversed between image perception and retrieval. The fusion analysis also suggests an information relay to frontoparietal areas late during retrieval. Together, the results shed light onto the temporal dynamics of memory recall and the transformations that the information undergoes between the initial experience and its later reconstruction from memory.

Key words: EEG; feature reconstruction; fMRI; memory retrieval; multivariate fusion

Significance Statement

We combined EEG and fMRI to investigate which features of a visual object are reactivated when recalled from episodic memory and how the memory reconstruction stream unfolds over time and across the brain. Our findings suggest that relative to perception, memory retrieval follows a backward information trajectory along a conceptual-to-perceptual gradient and additionally relays retrieved information to multimodal frontoparietal brain regions. These findings address the fundamental question of

Received March 4, 2024; revised July 3, 2024; accepted Aug. 9, 2024.

The authors declare no competing financial interests.

Author contributions: J.L.-C., J.L.-D., and Maria Wimber designed research; J.L.-C., B.J.G., J.L.-D., and C.S.F. performed research; J.L.-C., B.J.G., J.L.-D., C.S.F., Martin Wilson, S.D.M., I.C., and Maria Wimber analyzed data; J.L.-C. and Maria Wimber wrote the paper.

We thank Simrandeep Cheema, Dagmar Fraser, and Nina Salman for their help with data collection. We also thank Karen Mullinger for the useful analytical advice. This work was supported by a European Research Council (ERC) Starting Grant StG-2016-715714 awarded to Maria Wimber and a scholarship from the Midlands Integrative Biosciences Training Partnership (MIBTP) awarded to J.L.-D. The funders had no role in study design, data collection and interpretation, or the decision to submit the work for publication.

Continued on next page.

whether memories are more or less truthful reconstructions of past events or instead are subject to systematic biases that prioritize some types of features over others. Our data suggest that episodic memory retrieval is a dynamic and highly reconstructive process with clear prioritization of abstract–conceptual over detailed–perceptual information.

Introduction

Relative to visual perception, little is known about how the human brain reconstructs content that is retrieved from memory. We here investigated which features are preferentially reactivated where in the brain and when in time when visual objects are recalled from episodic memory.

Object perception triggers an information processing cascade along the ventral visual stream that follows a gradient of increasing abstraction: early processing stages are dominated by low-level perceptual representations, while later stages increasingly code for conceptual features (Kolb et al., 1995; Carlson et al., 2013; Cichy et al., 2014; Clarke and Tyler, 2015; Martin et al., 2018). After ~300 ms, information reaches the hippocampus, where concept cells represent objects as highly abstract, perceptually invariant concepts (Quiroga, 2012). The hippocampus presumably binds together information from different sources (including dorsal stream) and serves the longer-term storage and retrieval of associative information (Eichenbaum, 2001; Rolls, 2010; Danker et al., 2017).

Computational models assume that the hippocampus then uses partial reminders to recover the missing, associatively linked information, a process termed pattern completion (Marr, 1971; Teyler and DiScenna, 1986; O'Reilly and McClelland, 1994; Rolls, 2010, 2013). Pattern completion in turn dictates that neocortical brain regions reinstantiate the various features of the relevant event (Marr, 1971; Teyler and DiScenna, 1986; Teyler and Rudy, 2007; Rolls, 2013; Moscovitch, 2008), presumably leading to the subjective reexperiencing of a past event (Tulving et al., 1983).

These early computational models describe memory reinstatement as a noisy but in essence veridical process, where neocortical information is reestablished the way it was represented during initial perception. Evidence for copy-like encoding-retrieval-similarities (ERS) (Staresina et al., 2012) comes from neuroimaging studies using similarity- or classification-based multivariate analyses (Danker and Anderson, 2010; Rissman and Wagner, 2012; Staresina et al., 2012), showing reinstatement of individual episodes (Ferreira et al., 2019), scenes (Wing et al., 2014), semantic category (Polyn et al., 2005), sensory modality (Griffiths et al., 2019), or task context (Jiang et al., 2020). While these findings support the central premise that hippocampal pattern completion is associated with a more or less truthful reinstatement of encoding patterns, recent studies emphasize that information is not necessarily decodable from the same regions during encoding and retrieval (Favila et al., 2020; Xue, 2022). A shift in the location of content decoding from sensory to multimodal frontoparietal areas suggests a representational transformation between perception and memory recall, respectively (Xiao et al., 2017; Favila et al., 2018, 2020; Xue, 2022). This memory transformation may go along with a semanticization of the retrieved content (Favila et al., 2020), in which conceptual features become prioritized over low-level perceptual ones (Ferreira et al., 2019; Lifanov et al., 2021).

Due to the divergent previous findings, our first goal in the present study was to decompose visual object memories into perceptual and conceptual components and to test if both types of features are equally reinstated, in the same areas representing these features during encoding. Moving beyond spatial localization, we asked next how the neocortical reinstatement process unfolds over time, and whether different features of a memory are reactivated with different temporal priority. Such prioritization could naturally emerge from the hippocampus' differential connectivity with neocortical regions during retrieval. Once pattern completion is initiated, most information is relayed via the subiculum to the entorhinal cortex which in turn projects back to other cortical areas (Chrobak et al., 2000; Rolls, 2013; Staresina and Wimber, 2019). A majority of direct hippocampal and entorhinal efferents terminate in late areas of the visual processing hierarchy where representations cluster in abstract–semantic categories, while there are few connections to low-level sensory areas (Insausti and Muñoz, 2001; Dalton et al., 2022). We therefore expect that memories are initially reconstructed on a conceptual level, and that information coded in lower-level visual areas can only be reached at later stages of memory

Correspondence should be addressed to Maria Wimber at maria.wimber@glasgow.ac.uk or Julia Lifanov-Carr at jxl1118@alumni.bham.ac.uk.

reconstruction. Indeed recent studies using EEG decoding and behavioral responses demonstrated a temporal prioritization of conceptual over perceptual features during memory retrieval (Linde-Domingo et al., 2019; Lifanov et al., 2021), mirroring the hierarchy during perception of the same stimuli, similarly to mental imagery (Horikawa and Kamitani, 2017; Dijkstra et al., 2020). Whether the observed conceptual-to-perceptual gradient of feature recall truly maps onto a sensory backpropagation stream remains an open question.

The present study combined fMRI with EEG pattern analysis to test if recalling an object from memory elicits a backward processing cascade relative to perception. An associative recall paradigm with visual object stimuli (Linde-Domingo et al., 2019, Lifanov et al., 2021) allowed us to differentiate between perceptual and conceptual object features. First, based on fMRI patterns only, we compared where in the brain these low- and high-level feature dimensions can be decoded during retrieval as opposed to encoding. Second, using EEG–fMRI fusion to resolve spatial activation patterns in time, we asked whether the object information reconstructed during retrieval propagates backward (i.e., anterior to posterior) along the ventral visual stream, from high-level conceptual to low-level sensory areas.

Materials and Methods

Participants

We acquired fMRI data of 37 right-handed, fluent English-speaking participants at the University of Birmingham (26 females, 11 males, mean age (M_{age}) = 23.33, standard deviation (SD_{age}) = 3.89; one participant did not indicate their age). The a priori planned sample size for the full EEG–fMRI dataset was $n = 24$ subjects (as in Linde-Domingo et al., 2019). However, due to poor data quality and technical failures in 13 of the simultaneous EEG datasets, additional subjects were recorded leading to a larger sample size for the fMRI data alone. Three subjects were excluded from the fMRI analysis due to failed scanning sequences, and three additional subjects were excluded due to extensive motion within the scanner, exceeding the functional voxel size, such that 31 fMRI datasets remained for analysis. All participants were informed about the experimental procedure, underwent imaging safety screening, and signed an informed consent. The research (ethics code ERN_11-0429AP70) was approved by the STEM ethics committee of the University of Birmingham.

Due to poor data quality in the simultaneously acquired EEG set (see below, Analyses that did not work), we excluded the entire simultaneous EEG data from the analysis and instead used a previously published EEG dataset including the same stimulus set and a nearly identical associative learning and retrieval paradigm (Linde-Domingo et al., 2019). This additional dataset included 24 further participants with a clean, out-of-scanner EEG. For further information on the EEG data sample and the related ethical procedures, we refer to the previous work (Linde-Domingo et al., 2019).

Material

The paradigm was a visual verb–object association task (Linde-Domingo et al., 2019) adapted for fMRI in terms of timing. Stimuli included 128 action verbs and 128 pictures of everyday objects (Linde-Domingo et al., 2019). Action verbs were chosen because they do not elicit concrete object images in themselves but are still easy to associate with the object images. Importantly, all object images existed in two perceptual categories, a colored photograph from the BOSS database (Brodeur et al., 2010, 2014) or a black line drawing version of a respective photograph created by Linde-Domingo et al. (2019) by means of the free and open-source GNU Image Manipulation Program (GIMP) software (The GIMP Development Team, 2019). Furthermore, each object belonged to one of the two conceptual categories, i.e., animate versus inanimate. We selected 128 images per participant according to a fully balanced scheme, such that each combination of perceptual and conceptual categories included the same number of pictures (32 animate photographs, 32 animate drawings, 32 inanimate photographs, 32 inanimate drawings; Fig. 1*a*). With respect to the later fusion with the out-of-scanner EEG data, it is important to note that while both experiments used the same set of 128 objects, the same object could appear in different perceptual versions between participants, due to the pseudorandomized image selection. For example, an image of a camel could be shown as a photograph to one participant and as a line drawing to another. Action verbs were randomly assigned to images in each participant and were presented together with pictures centrally overlaid on a white background.

Procedure

Before the session, participants were informed about the experimental procedure and asked to perform a training task block in front of the computer. After completion of the training, the experimental session in the fMRI scanner included four runs with four task blocks each, summing up to a total of 16 task blocks. A typical block in the training and experimental task included the encoding of eight novel associations, a 20 s distractor task, and 16 retrieval trials (two repetitions per association). A 3 min break was included after each fMRI run, in which participants were asked to rest and close their eyes. In total, it took participants ~70 min to perform the entire task.

Encoding

In the encoding phases (Fig. 1*b*), participants were instructed to study eight novel verb–object pairings in a random order. A trial started with a fixation cross presented for a jittered period between 750 and 2,500 ms. The action verb was presented for 500 ms before an object was shown for a maximum duration of 6 s. To facilitate learning, participants

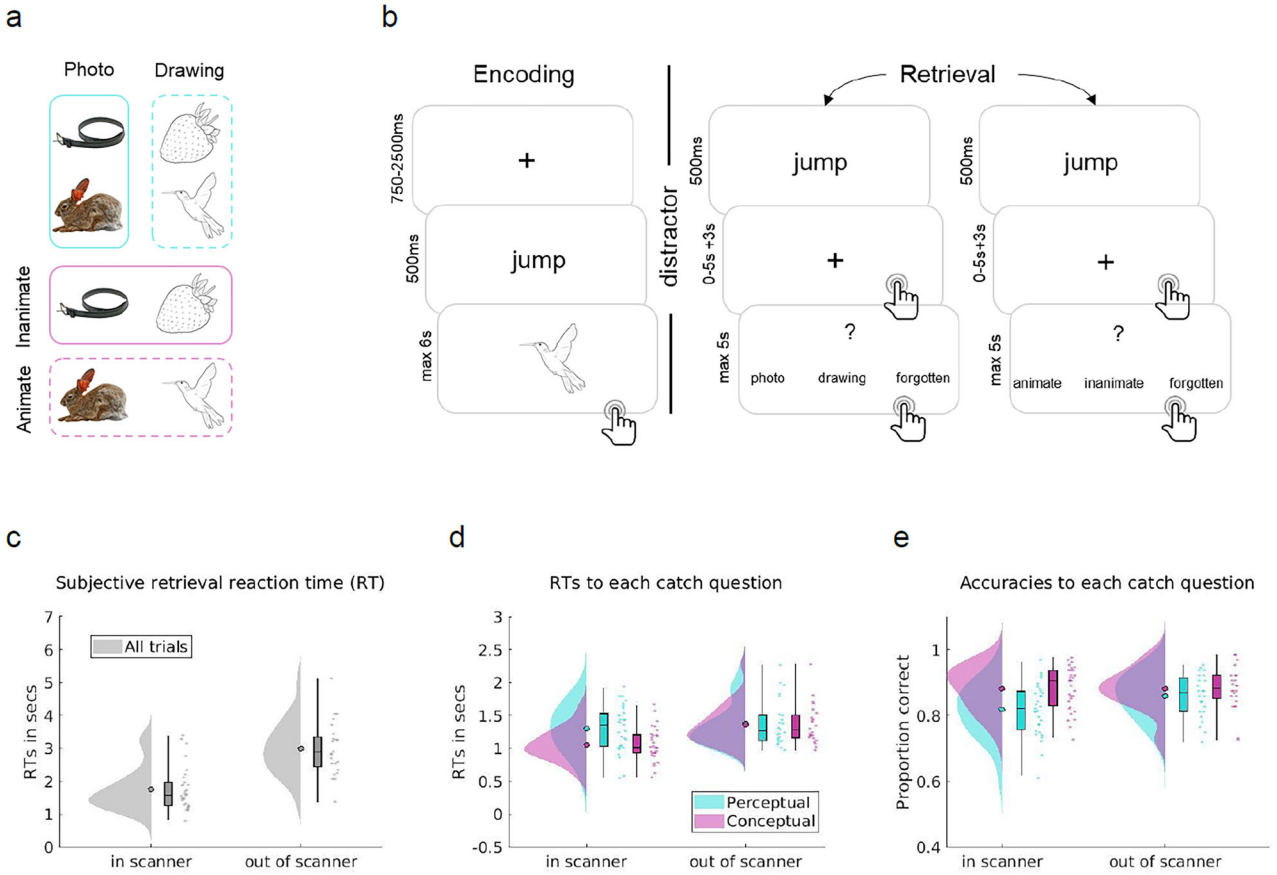

Figure 1. Overview of stimuli and task. ***a***, Design of the stimuli. The 128 pictures used in any given participant were orthogonally split into 64 drawings and 64 photographs, out of which 32 were animate and 32 inanimate objects, respectively. Each object could thus be classified along a perceptual (photo/drawing, cyan) or conceptual (animate/inanimate, magenta) dimension. ***b***, One prototypical task block of the paradigm. At encoding, participants were asked to associate verb–object pairings and indicate the successful formation of an association by button press. After a 20 s distractor task, participants did a memory test where on each trial, they recalled the previously associated object upon presentation of a verb cue and indicated successful subjective recollection by button press (referred to as retrieval button press). Then participants were asked to hold the mental image of the object in mind for a further 3 s, before answering a perceptual or conceptual catch question. Each association was tested twice during retrieval, once with a perceptual, and once with a conceptual question, with several intervening test trials in between repetitions of the same association. Participants performed 16 task blocks overall, with eight novel associations per block. Stimuli illustrated are chosen from the BOSS database (Brodeur et al., 2010, 2014; https://creativecommons.org/licenses/by-sa/3.0/, Photos: Copyright © 2014 Brodeur et al.) and customized with free and open-source GIMP software (The GIMP Development Team, 2019; https://www.gimp.org; Linde-Domingo et al., 2019). Figure adapted from Lifanov et al. (2021) and Linde-Domingo et al. (2019). ***c–e***, Behavioral data acquired within (EEG–fMRI group) and out of scanner (EEG only group). ***c***, Subjective retrieval RTs, ***d***, RTs for each type of catch question. ***e***, Catch question accuracies for the two question types. Filled circles represent the overall *M*; boxplots represent median and 25th and 75th percentiles; whiskers represent 2nd and 98th percentile; dots represent the *M* of individual subjects. Gray represents all trials; cyan represents responses to perceptual and magenta to conceptual questions. In-scanner data come from $n = 31$ independent subjects, out-of-scanner data from $n = 24$ independent subjects. Figures made using RainCloud plots Version 1.1 (https://github.com/RainCloudPlots/RainCloudPlots, M. Allen et al., 2018, 2021).

were instructed to form a vivid visual mental image using the verb–object pairing and, once formed, to press a button with their thumb, which moved the presentation on to the next trial. Importantly, due to the artificial setting where there is no predictive structure to the events, we expected very limited top–down feedback and hence a dominating feedforward sweep during perception early on.

Distractor

After each encoding phase, participants performed a self-paced distractor task for 20 s, indicating as fast as possible whether each of the consecutively presented numbers on the screen was odd or even, pressing a button with their index or middle finger, respectively. Feedback on the percentage of correct responses was provided at the end of each distractor phase.

Retrieval

In the retrieval phases, participants were instructed to recall the previously associated objects upon presentation of the corresponding verb (Fig. 1*b*). Trials started with the presentation of a fixation cross, jittered between 500 and 1,500 ms and

followed by a previously encoded action verb, presented for 500 ms. Cued with the verb, participants were instructed to recall the paired object within a maximum of 5 s, while a black fixation cross was presented on the screen. Note that this maximum duration was shorter than in the original task (Linde-Domingo et al., 2019), which might have caused participants to react faster and possibly explains reaction time (RT) differences between the in-scanner and out-of-scanner datasets (Fig. 1c). Participants were asked to indicate the time point of image recall by button press with their thumb, at which point the black fixation cross turned gray and was presented for an additional 3 s. This retrieval button press was meant to mark the time point of subjective recollection. During the remaining 3 s, participants were asked to hold the mental image of the object in mind as vividly as possible. Last, they were asked about the perceptual (was the object a photograph or a line drawing?) or conceptual (was the object animate or inanimate?) features of the recalled object, answering with their index or middle finger within a maximum response period of 5 s. During the presentation of the catch question, participants also had the option to indicate with their ring finger that they forgot the features of the corresponding object. Importantly, each encoded stimulus was retrieved twice, once with a perceptual and once with a conceptual question. Trial order was pseudorandom within the first and second set of repetitions, with a minimum of two intervening trials before a specific object was recalled for the second time. The order of catch questions was counterbalanced across repetitions such that half of the associations were first probed with a perceptual question, and the other half was first probed with a conceptual question.

fMRI data acquisition

FMRI scanning was performed in a 3 Tesla Philips Achieva MRI scanner with a 32-channel SENSE head coil at the Birmingham University Imaging Centre (now the Centre for Human Brain Health). Slices covered the whole head. T1-weighted anatomical scans were collected with an MP-RAGE sequence [1 mm isotropic voxels; 256 × 256 matrix; 176 slices; no interslice gap; repetition time (TR), 7.5 ms; field of view (FOV), 256 × 256 × 176 mm; flip angle (FA), 7°; echo time (TE), 3.5 ms]. T2*-weighted functional images were acquired by a dual-echo EPI pulse sequence with a low specific absorption rate to optimize the image quality in regions highly susceptible for distortions by a long readout gradient (3 × 3 × 3.5 mm; 64 × 64 matrix; 34 slices; no interslice gap; TR, 2.2 s; full head coverage; FOV, 192 × 192 × 119 mm; FA, 80°; TE1, 12 ms; TE2, 34 ms; for dual-echo information, see also Halai et al., 2014, 2015; Kirilina et al., 2016). Slices were acquired in a continuous descending fashion. Furthermore, we collected 200 resting-state volumes, 50 after each of the four task runs, used for the later combining of dual-echo images with the short and long TEs. During the acquisition of the functional scans, the helium pump was switched off to prevent contamination of the EEG by the compressor artifact at ∼20–30 Hz. Stimulus timings were jittered in relation to the acquired scans. The task was presented to participants through a mirror system in the scanner and a JVC SX 21e projector with resolution 1,280 × 1,024 at 60 Hz (https://de.jvc.com/). Participants' heads were extra padded to minimize movement artifacts. The stimulus presentation, and the collection of timing and accuracy information, was controlled by scripts written in MATLAB (The MathWorks Inc., 2016, https://www.mathworks.com) and Psychophysics Toolbox (Brainard, 1997; Pelli, 1997; Kleiner et al., 2007; version 3). Responses were logged by NATA response boxes (https://natatech.com/).

Out-of-scanner EEG data acquisition

As previously stated, a simultaneous EEG dataset was acquired during the fMRI session, but this EEG dataset was too noisy to decode retrieval-related information. We therefore decided to instead use an out-of-scanner EEG dataset for data fusion. This out-of-scanner data, used for all analyses reported here, originated from a previous publication (Linde-Domingo et al., 2019). We give a short description of the EEG data acquisition in the following and of the EEG preprocessing further below. More details can be found in the original publication.

For EEG data collection, 128 electrodes of silver metal and silver chloride were used. Furthermore, an Active-Two amplifier system and the ActiView acquisition software aided data recording (BioSemi; https://www.biosemi.com/). Psychophysics Toolbox (Brainard, 1997; Pelli, 1997; Kleiner et al., 2007; version 3) and MATLAB (The MathWorks Inc., 2014, https://www.mathworks.com) were used for task presentation and response collection (Linde-Domingo et al., 2019).

Analyses

Behavior

Behavioral data were analyzed by MATLAB (The MathWorks Inc., 2017, https://www.mathworks.com). For the inspection of RTs and accuracies, the behavioral data were preprocessed as follows. For the RT analysis, all trials with incorrect responses to the catch question were removed first. Additionally, catch question RTs of correct trials were removed if they were faster than 200 ms or exceeding the average RT of a participant in a given set of repetitions (first or second cycle) by more than three times the SD (Linde-Domingo et al., 2019; Lifanov et al., 2021). For the analysis of the accuracy data, trials faster than 200 ms and objects with a missing response for either of the two questions were excluded in the corresponding cycle (Lifanov et al., 2021). The same procedures were applied to the data of the out-of-scanner EEG participants, who performed a nearly identical task. However, note that out-of-scanner EEG participants only went through one cycle of retrieval.

FMRI data preprocessing

We used MATLAB (The MathWorks Inc., 2017, https://www.mathworks.com) and SPM 12 (Penny et al., 2007) for the preprocessing and the analysis of fMRI data. All functional images were first realigned based on three motion and three rotation parameters, unwarped, and slice time corrected to the middle slice in time.

After these initial preprocessing steps, images obtained during the task at two echo times were combined as a weighted average (Poser et al., 2006). Importantly, the relative weights were obtained from the SNR of 200 resting-state volumes per echo and its corresponding TE as follows:

$$w(\mathrm{CNR})_n = \frac{\mathrm{SNR}_n * \mathrm{TE}_n}{\sum_n \mathrm{SNR}_n * \mathrm{TE}_n}, \quad (1)\ \text{(equation from Poser et al., 2006)}$$

where w is the weight for an individual voxel, SNR_n is the signal-to-noise ratio here calculated as ratio of M to SD of the given voxel calculated over time at the nth echo, and TE is the readout time of the nth echo.

Weights obtained from the resting state were then used to combine task volumes from both echoes as follows:

$$S = w_1 * S_1 + w_2 * S_2, \quad (2)\ \text{(as described by Poser et al., 2006)}$$

where S is the final signal of an individual voxel over time, calculated by summing the weighted signals of both echoes. These methods and equations were applied as described in work on BOLD contrast optimization by multiecho sequences (Poser et al., 2006). Combined image structures were written to NIFTI files (https://nifti.nimh.nih.gov/) by Tools for NIfTI and ANALYZE image (Shen, 2014, https://www.mathworks.com/matlabcentral/fileexchange/8797-tools-for-nifti-and-analyze-image).

Anatomical images were segmented, coregistered with the functional images, and normalized into a standard MNI template in SPM 12 (Penny et al., 2007). Then, after the combination of functional images, the T2* images were also normalized into MNI space, using the T1-based normalization parameters. Finally, EPI images were smoothed for the univariate GLM analysis with a Gaussian spatial filter of 8 mm full-width at half-maximum (FWHM). Note that multivariate analyses were performed on unsmoothed data in native space (Weaverdyck et al., 2020).

ROIs. Regions of interest (ROIs) were created from templates in MNI space as available in the WFU PickAtlas v3.0 (Lancaster et al., 1997, 2000; Tzourio-Mazoyer et al., 2002; Maldjian et al., 2003, 2004). These ROIs were then fitted to individual brains by applying the reversed T1-based normalization parameters (see above, FMRI data preprocessing) to the ROI masks (as in Chang and Glover, 2010). To define the anatomical masks, we used Brodmann areas (BAs, Brodmann, 1909) from the Talairach Daemon database atlases (Lancaster et al., 1997, 2000) and automated anatomical labeling (AAL, Tzourio-Mazoyer et al., 2002). The anatomical masks used for our analyses included an early visual mask (V1/V2), consisting of BAs 17 and 18; a human inferior temporal (hIT) mask, consisting of BAs 19 and 37; a temporal pole mask, consisting of superior and middle temporal pole regions as defined by AAL; a medial temporal lobe (MTL) mask, consisting of BAs 28, 34, 35, and 36 and AAL rhinal sulcus and parahippocampal gyrus; a superior parietal lobe mask, consisting of BA 7; a lateral (inferior) parietal lobe mask, consisting of BAs 39 and 40; and a medial parietal lobe mask, consisting of BAs 29 and 30.

EEG data preprocessing

EEG data (Linde-Domingo et al., 2019; see section "Data availability") were preprocessed in the MATLAB (The MathWorks Inc., 2014, https://www.mathworks.com) and the FieldTrip toolbox (Oostenveld et al., 2010; Donders Institute for Brain, Cognition and Behaviour, Radboud University Nijmegen, the Netherlands. See http://www.ru.nl/neuroimaging/fieldtrip, version from 3 Aug. 2017). During epoching, different temporal references were used for encoding and retrieval. Encoding epochs were stimulus locked to the onset of the object image, while retrieval timelines were locked to the subjective retrieval button press, in order to observe the reactivation stream leading up to the subjective experience of recollection. These epochs were created with a length of 2 s (−500 before to 1,500 ms after object onset) for encoding and 4.5 s (−4 s before to 500 ms after retrieval button press) for retrieval. Line noise was removed by a finite impulse response filter with a band-stop between 48 and 52 Hz. A high-pass filter with a cutoff frequency of 0.1 Hz was applied to remove slow temporal drifts and a low-pass filter with a cutoff frequency of 100 Hz to remove high-frequency noise. Individual artifactual trials and bad electrodes were rejected manually. Remaining artifacts were removed by independent component analysis, after which any excluded electrodes were reintroduced by interpolation. The referencing of the data was set to the average across all scalp channels.

After this step, we implemented additional preprocessing steps using MATLAB (The MathWorks Inc., 2017, https://www.mathworks.com) and the FieldTrip toolbox (Oostenveld et al., 2010; Donders Institute for Brain, Cognition and Behaviour, Radboud University Nijmegen, the Netherlands. See http://www.ru.nl/neuroimaging/fieldtrip, version from 16 November 2017) to prepare data for the specific fusion analyses of this paper. The encoding data were baseline corrected by subtracting the average signal in the prestimulus period (−0.2 to −0.1 s) for all poststimulus time points, separately per electrode. The retrieval data were baseline corrected by whole-trial demeaning, since retrieval trials had no

obvious, uncontaminated baseline period. The EEG time series data were then downsampled to 128 Hz and temporally smoothed with a moving average with a time window of 40 ms.

fMRI univariate analyses

We first performed a univariate GLM analysis and subsequent *t*-contrasts on the fMRI data to reveal activation differences between the two perceptual and the two conceptual categories (Extended Data Fig. 2-2, Extended Data Tables 2-7–2-9). The GLM included the four main regressors (drawing-animate, photograph-animate, drawing-inanimate, and photograph-inanimate), with separate regressors for encoding, first retrieval, and second retrieval, using all trials. We used stick functions locked to the object onset to model encoding trials and boxcar functions with a duration of 2.5 s locked to the cue onset to model retrieval trials. We added one regressor each for the presentation of verbs, button presses, and perceptual and conceptual catch questions as well as nuisance regressors for head motion, scanner drift, and run means. After computing the GLM for each subject, a sample-level ANOVA was computed with the perceptual (photograph vs line drawing) and conceptual (animate vs inanimate) dimensions as within-subject factors. Planned comparisons contrasting photographs versus drawings and animate versus inanimate objects were carried out in subsequent *t*-contrasts separately at encoding and retrieval for all trials. The *t*-contrasts for retrieval trials were performed using both the first and second retrieval trials together.

fMRI multivariate analyses

As preparation for the multivariate analyses, we performed a GLM, modeling individual object-specific regressors for encoding, and, for each of the two retrieval repetitions separately, adding regressors of no interest for the presentation of verbs, button presses, and catch question onsets, as well as nuisance regressors for head motion, scanner drift, and run means (one regressor per variable containing all onsets; Griffiths et al., 2019). We used stick functions locked to the object onset to model encoding trials and boxcar functions with a duration of 2.5 s locked to the cue onset to model retrieval trials. The resulting beta weights were transformed into *t* values for all subsequent multivariate analyses (Misaki et al., 2010).

fMRI searchlight LDA. To investigate where in the brain activity patterns differentiated between the two perceptual and the two conceptual categories, we performed a volumetric linear discriminant analysis (LDA) searchlight analysis on the non-normalized and unsmoothed fMRI data of each participant individually using the searchlight function of the representational similarity analysis toolbox (RSA, Nili et al., 2014; https://www.mrc-cbu.cam.ac.uk/methods-and-resources/toolboxes/). The LDA was calculated using the MVPA-Light toolbox (Treder, 2020; https://github.com/treder/MVPA-Light). This was done at each center voxel of a sphere, where object-specific *t* values of the voxels within a 3D searchlight radius of 12 mm were used as feature vectors. Using these feature vectors, we classified perceptual (photo vs drawing) and conceptual (animate vs inanimate) categories by a fivefold LDA with five repetitions, preserving class proportions, separately for encoding and retrieval using all trials. Individual accuracy maps were normalized to MNI space and spatially smoothed with a 10 mm FWHM Gaussian kernel, before second-level *t* tests were performed to statistically compare voxel-specific classification accuracies against 50% chance performance. Finally, the results were plotted on an MNI surface template brain.

fMRI correlation-based RSA. As preparation for the fusion of EEG and fMRI data, we performed an RSA (Kriegeskorte et al., 2006, 2008; Kriegeskorte, 2009; Kriegeskorte and Kievit, 2013; Nili et al., 2014; https://www.mrc-cbu.cam.ac.uk/methods-and-resources/toolboxes/) on the non-normalized and unsmoothed fMRI data. FMRI-based *t*-maps corresponding to unique objects were arranged in the same order for all participants. As mentioned earlier, object correspondence across participants was only given on the level of object identity (and thus also conceptual category), but not perceptual format. In other words, all participants saw an image of a camel (i.e., an animate object) at some point in the experiment, but the camel could be presented as a photograph to some participants and as a line drawing to others. For each voxel and its surrounding neighbors within a radius of 12 mm, we extracted object-specific *t* value patterns resulting from the appropriate GLM and arranged these as one-dimensional feature vectors. Using these feature vectors, we calculated the Pearson's correlation distance ($1 - r$) between each pair of objects at each voxel location, separately for encoding and retrieval. The resulting representational dissimilarity matrix (RDM) maps were saved and used at a later stage for the searchlight fusion with the EEG data.

In a similar fashion to the searchlight approach, RDMs were also calculated for the predefined set of anatomical ROI in the non-normalized and unsmoothed individual functional datasets (see above, ROIs). The resulting ROI RDMs were used at a later stage for the ROI fusion.

EEG multivariate analyses

Our next step was to construct an RDM for each time point of the EEG recordings, resulting in one timeline representing the similarity structure of our object dataset across all subjects. Cells of the RDM represented the pairwise discriminability of object pairs, based on a cross-subject classification of object identity using the MVPA-Light toolbox (Treder, 2020; https://github.com/treder/MVPA-Light). To compute this matrix, we arranged object-specific trials in the same order

between all participants, independent of their perceptual format, and up to 24 repetitions of each individual object across participants were used for the pairwise classification (note that after trial removal in the preprocessing, an average of $M = 3.09$ trials per object were missing in the encoding and $M = 3.93$ trials per object were missing in the retrieval data). Specifically, we performed a time-resolved LDA using as feature vectors the EEG amplitude values from the 128 electrodes, at a given time bin, and participants as repetitions of the same object. To tackle problems of overfitting, we used automatic shrinkage regularization as implemented in the MVPA-Light toolbox (Treder, 2020, https://github.com/treder/MVPA-Light). We used the LDA to classify object identity among each pair of objects at each time bin, again with a fivefold cross-validation, preserving class proportions. The resulting discrimination accuracies were entered in a single time-resolved RDM structure representing the dissimilarity between individual objects of our stimulus pool across participants over time. This classification procedure was performed independently for encoding and retrieval.

Before using the EEG-based RDMs for our data fusion, we also wanted to assess statistically how much information about object identity can be decoded from the EEG signals themselves. We therefore first calculated the average classification performance across all pairwise accuracies as a descriptive measure. We then tested if the pairwise accuracies resulting from the "real" classification with correct object labels were significantly larger than the pairwise accuracies that resulted from a classification with permuted object labels. This test was performed in two steps. First, we created 25 classification-based RDMs (same classification procedure as for the "real" RDM time course) but each one with randomly permuted object labels, keeping a given label permutation consistent across time in order to preserve the autocorrelation of the EEG time series. The 25 permutations were averaged to form a single "baseline" RDM time course.

As a second step, we used a cluster-based permutation test to find clusters with temporally extended above-chance decoding accuracy. This cluster-based permutation test compared the *t*-statistic of each time point resulting from a "real matrix" versus "baseline matrix" *t* test with the *t*-statistics computed from a "real matrix" versus "baseline matrix" *t* test, this time shuffling the "real" and "baseline" cells between the two matrices (consistent shuffling across time, independent samples *t* test to control for unequal variance, 1,000 permutations, cluster-definition threshold of $p < 0.05$, as used in previous publications; Cichy and Pantazis, 2017; Cichy et al., 2019; Dobs et al., 2019). Note that the variance in the *t* tests for each time bin comes from the pairwise accuracies contained in the cells of the two ("real" and "baseline") classification matrices. All remaining analyses were performed using the ("real") classification matrix with the correct object labels.

Next, we tested whether object discriminability systematically differs between objects coming from the same or different conceptual classes (i.e., animate and inanimate objects) within the classification with correct labels. We thus calculated the average accuracies of pairwise classes within and between conceptual categories as a descriptive measure. Using another cluster-based permutation test (paired-sample *t* test, 1,000 permutations, cluster-definition threshold of $p < 0.05$), we statistically tested for differences of within- against between-category accuracies over time. This analysis was conducted for conceptual classes only, as there was no correspondence of perceptual class between subjects. The encoding analyses focused on the time period from 0 to 1.5 s after the object onset, while the retrieval analyses focused on the time period from −3 to −1 s before retrieval button press. We based this latter time window of interest on previous findings (Linde-Domingo et al., 2019) which indicated perceptual and conceptual decoding peaks prior to −1 s before button press. All cluster permutation tests were implemented by means of the permutest toolbox (Gerber, 2019, https://www.mathworks.com/matlabcentral/fileexchange/71737-permutest; Maris and Oostenveld, 2007).

EEG–fMRI data fusion

ROI fusion. Two distinct approaches were used for the fusion analyses, with either the fMRI data or the EEG data serving as starting point. The first approach used the fMRI patterns from a given ROI as a starting point, and we thus refer to it as ROI fusion. One RDM was created per participant per ROI, representing the similarity structure (i.e., RDM) in a given anatomical brain region. This ROI RDM was then Spearman's-rank-correlated with the RDM from each time bin of the single, EEG-based RDM time course that represents the pooled similarity structure across subjects (see cross-subject classification described above). Correlations and classification accuracies were Fisher's *z*-transformed before the data fusion (as in Griffiths et al., 2019). This analysis resulted in one correlation time course per individual ROI per subject who took part in the fMRI experiment ($n = 31$). The EEG–fMRI correlations were only computed for those cells of the matrix that an individual participant from the fMRI study remembered correctly. To test for statistical significance, we then contrasted the 31 correlation time courses against zero, using a cluster-based permutation test with 1,000 permutations and a cluster-definition threshold of $p < 0.05$, correcting for multiple comparisons in time as in previous studies (Cichy and Pantazis, 2017; Cichy et al., 2019; Dobs et al., 2019).

To test for a sequential information progression over the ventral visual stream regions, we implemented a linear regression on the cumulative sums of the ROI time courses (Michelmann et al., 2019). This analysis complements the ROI fusion approach and was designed specifically to detect a cascade of serial processing stages, applied here to the representational similarity across a specific order of ROIs. Furthermore, it has been shown to be a strong method to identify such cascades within participants (Michelmann et al., 2019). To do so, we first calculated the cumulative sum of the ROI time courses over the time period from 0 to 1.5 s after the image onset for encoding and from −3 to −1 s before button press for retrieval. To compensate for total correlation differences between ROIs and make them more comparable, the cumulative sum of each ROI time course was normalized to an area under the curve that equals 1 (Michelmann

et al., 2019). For each time point, a linear regression was fitted across the cumulative correlation values of the ROIs within subjects. The resulting slopes of all subjects were then tested against zero in a one-sided cluster–based permutation test (with 1,000 permutations and a cluster-definition threshold of $p < 0.05$). This method enabled us to test for a forward stream during encoding and a backward stream during retrieval (Fig. 4*e*,*f*). An example of the rationale is illustrated in Figure 3. In the case of a forward stream, the ROIs along the ventral visual stream activate sequentially from early toward late regions. Therefore, earlier regions (e.g., V1-hIT) show a higher cumulative sum than later regions (e.g., temporal pole—MTL) at 0.5 s after the stimulus onset (and other time points). A linear fit across ROIs at 0.5 s will therefore show a significant negative slope. According to this rationale, a backward stream across the same regions would result in a significant positive slope, while data peaks merely based on noise would reveal a slope near zero. Since we expected a forward stream at encoding and a backward stream at retrieval, we used one-sided tests to confirm if the slope differs from zero (<0 at encoding, >0 at retrieval). The sequential ordering of our ROIs was based on literature describing the hierarchical organization of the ventral visual stream in anatomical and functional neuroimaging studies (Felleman and Essen, 1991; Clarke et al., 2013; Cichy et al., 2014, 2016, 2017; Leonardelli and Fairhall, 2022).

Searchlight fusion. The second, complementary fusion approach offers higher spatial resolution and a whole-brain perspective on how encoding and retrieval patterns emerge over time. Here, we used the EEG-based RDMs from each time point as starting point and then searched for matching similarity structures across the entire brain, using a volumetric searchlight analysis on each individual's fMRI data (Kriegeskorte et al., 2006, 2008; Kriegeskorte, 2009; Kriegeskorte and Kievit, 2013; Nili et al., 2014, https://www.mrc-cbu.cam.ac.uk/methods-and-resources/toolboxes/). We refer to this method as a (time-resolved) searchlight fusion. A second-order correlation was computed between the (classification-based) EEG RDM from each time bin and the (correlation-based) fMRI RDMs for each center voxel and its neighbors within a searchlight radius of three voxels, separately for encoding and retrieval. This analysis results in a "fusion movie" (i.e., a time-resolved brain map) for each participant who took part in the fMRI experiment. The searchlight fusion for retrieval data was performed for correct trials within the fMRI data only (same as above). The fused data was Fisher's *z*-transformed. The searchlight fusion was performed using the Python Representational Similarity Analysis toolbox (RSA Group, 2019, https://rsatoolbox.readthedocs.io/en/latest/, https://github.com/rsagroup/rsatoolbox) written in Python (van Rossum, 1995), using the sys and os module, SciPy (Virtanen et al., 2020a,b), NumPy (Harris et al., 2020), and nibabel (https://nipy.org/nibabel/; https://github.com/nipy/nibabel/releases).

To test for significant EEG–fMRI pattern similarity at individual voxels, we normalized the correlation maps to MNI space, smoothed them with a 10 mm FWHM Gaussian kernel and then tested them in a one-sample *t* test against zero at each single time bin. The *t* test included a spatial maximal permuted statistic correction combined with a threshold-free cluster enhancement (Nichols and Holmes, 2002; Smith and Nichols, 2009). This cluster-based analysis was performed using the toolbox MatlabTFCE (Thornton et al., 2016, http://markallenthornton.com/blog/matlab-tfce/) with 1,000 permutations, a height exponent of 2, an extent exponent of 0.5, a connectivity parameter of 26, and a step number for cluster formation of 0.1 as suggested by Smith and Nichols (2009). The analysis resulted in time-resolved spatial *t*-maps, depicting clusters of significant EEG–fMRI correlations, created by Tools for NIfTI and ANALYZE image (Shen, 2014, https://www.mathworks.com/matlabcentral/fileexchange/8797-tools-for-nifti-and-analyze-image).

Figures

Figures were created using SPM 12 (Penny et al., 2007), the RainCloud plots (M. Allen et al., 2018, 2021, https://github.com/RainCloudPlots/RainCloudPlots), Inkscape (Inkscape Project, 2020), WFU PickAtlas v3.0 (Maldjian et al., 2003, 2004), MRIcron (Rorden and Brett, 2000, https://www.nitrc.org/projects/mricron, www.mricro.com), and a Colin 27 average brain template (Holmes et al., 1998, http://www.bic.mni.mcgill.ca/ServicesAtlases/Colin27).

Analyses that did not work

Data fusion with the in-scanner EEG

The initial plan for this project was to fuse the fMRI data with the EEG data acquired during scanning. Using the simultaneous EEG data for fusion, the spatiotemporal mapping could then have been performed on a trial-by-trial basis within participants. However, neither a time-resolved RSA nor a perceptual or conceptual LDA classification on the EEG data showed interpretable results, likely due to extensive remaining scanner artifacts in the in-scanner EEG data. As shown previously, head movement during simultaneous fMRI acquisition contributes noise signal in the EEG recordings, particularly within a frequency range under 20 Hz (Fellner et al., 2016). This becomes especially problematic for information decoding, given the importance of signals in the theta band (3–7 Hz) and below for decoding stimulus content (Vidaurre et al., 2021).

Data fusion with correlation-based EEG RDMs

Having decided to use the out-of-scanner EEG dataset for the data fusion, we first attempted to perform the fMRI-EEG fusion using correlation-based RDMs calculated from the EEG data (Cichy and Oliva, 2020). To compute these RDMs, we arranged object-specific trials in the same order between all participants, independent of their perceptual format, identical

to the arrangement in the fMRI data. We then performed a time-resolved RSA using EEG amplitude values from the 128 electrodes, at a given time bin, as feature vectors. Specifically, we calculated the pairwise distance [1 – correlation (*r*)] between each pair of objects. However, inspecting the average overall similarity and contrasting the average similarity within versus between conceptual classes did not show interpretable results. This is most likely due to too unreliable and time-varying single–trial estimates from the EEG data. Following this initial analysis, we thus used the cross-subject, classification-based RDMs that produced more stable results on the EEG data itself.

Results

In our memory paradigm, based on Linde-Domingo et al. (2019), participants first encoded novel associations between objects and action verbs. Importantly, object images varied along a perceptual (photographs vs line drawings) and a conceptual (animate vs inanimate) dimension that were used for later classification to distinguish between the two hierarchical processing levels. At the recall stage, following a distracter task, participants were asked to retrieve the object in as much detail as possible when presented with the verb and to indicate the time point of subjective recall with a button press while holding the retrieved image in mind. Following this subjective button press, participants answered either a perceptual (was the object a photograph/drawing?) or conceptual (was the object animate/inanimate?) question on each recall trial. Using this paradigm in an fMRI environment, we aimed at pinpointing the retrieval-related reinstatement of different object features in the brain. A searchlight classification approach was used to spatially locate perceptual (photograph vs drawing) and conceptual (animate vs inanimate) representations during image encoding and retrieval. The next aim was to map spatial representations onto a precise timeline preceding the subjective recall button press on a trial-by-trial basis within subjects, using simultaneous EEG–fMRI data acquisition. Since the within-scanner data turned out to be too noisy to decode the relevant object features (see Materials and Methods, Analyses that did not work), we instead used a previously acquired out-of-scanner EEG dataset (Linde-Domingo et al., 2019) to map the spatial representations onto the memory reconstruction timeline. This was done by means of an EEG–fMRI data fusion, using a second-order RSA (Kriegeskorte et al., 2006, 2008; Kriegeskorte, 2009; Kriegeskorte and Kievit, 2013; Nili et al., 2014).

Behavior

We first analyzed the behavior of participants who completed the fMRI study and descriptively compared their performance with the participants who took part in the out-of-scanner EEG study (Linde-Domingo et al., 2019). The in- and out-of-scanner encoding data showed comparable RTs and accuracy rates (Table 1). However, looking at subjective retrieval RTs (Fig. 1*c*), participants in the fMRI study were 1.24 s faster on average to indicate subjective retrieval than participants in the EEG study. This RT difference was not only a result of the repeated retrievals in the fMRI group, since RTs of both the first ($M1 = 1.93$ s; SD1 = 0.67 s) and second ($M2 = 1.58$ s; SD2 = 0.66 s) retrieval repetition of the fMRI group were substantially shorter than those of the EEG group. Participants in the fMRI sample might thus have tended to indicate subjective retrieval prematurely, possibly due to discomfort in the scanner environment, and this may have had knock-on effect on the catch question RTs discussed in the next paragraph.

After an explorative inspection of the behavioral data, we compared accuracies and RTs between perceptual and conceptual catch questions using paired-sample *t* tests (Table 2). Note that, different from our previous behavioral work (Linde-Domingo et al., 2019; Lifanov et al., 2021), the paradigm used here was optimized for capturing neural retrieval patterns rather than measuring feature-specific reaction times. After cue onset, participants were first instructed to mentally

Table 1. *M* and SD of encoding and subjective retrieval RTs and accuracies of in- and out-of-scanner data

	In-scanner	Out-of-scanner
Encoding RT	$M = 3.03$ s; SD = 0.90 s	$M = 2.82$ s; SD = 1.56 s
Retrieval RT	$M = 1.75$ s; SD = 0.66 s	$M = 2.99$ s; SD = 0.81 s
Retrieval accuracy	$M = 84.58\%$; SD = 0.07	$M = 86.75\%$; SD = 0.06

Table 2. *M* and SD of RTs and accuracies for perceptual and conceptual questions separately of (a) in- and (b) out-of-scanner data and paired-sample *t* test between perceptual and conceptual performances (see Extended Data Tables 2-7–2-9 for univariate and Extended Data Tables 2-3–2-6b for multivariate fMRI results)

	RTs	Accuracy
(a) In-scanner		
Perceptual	$M = 1.30$ s; SD = 0.35 s	$M = 0.82$; SD = 0.08
Conceptual	$M = 1.06$ s; SD = 0.25 s	$M = 0.88$; SD = 0.07
t test	$t_{(30)} = 8.47$; CI = [0.18, 0.30]; $p < 0.001$ (unc.)	$t_{(30)} = -6.49$; CI = [−0.08, −0.04]; $p < 0.001$ (unc.)
(b) Out-of-scanner		
Perceptual	$M = 1.38$ s; SD = 0.35 s	$M = 0.86$; SD = 0.07
Conceptual	$M = 1.36$ s; SD = 0.30 s	$M = 0.88$; SD = 0.07
t test	$t_{(23)} = 0.5$; CI = [−0.06, 0.10]; $p = 0.62$ (unc.)	$t_{(23)} = -1.80$; CI = [−0.05, 0.00]; $p = 0.09$ (unc.)

reinstate the object and indicate retrieval by button press. At this stage, we expected participants to have a fully reconstructed image of the recalled object in mind, such that answering the perceptual and conceptual catch question afterward would take equally long. In the EEG study (Linde-Domingo et al., 2019), participants indeed answered conceptual and perceptual questions equally fast [$t_{(23)} = 0.5$; $p = 0.62$ (unc.)] and accurately [$t_{(23)} = -1.80$; $p = 0.09$ (unc.)]. Participants in the fMRI study, however, performed less accurately [$t_{(30)} = -6.49$; $p < 0.001$ (unc.)] and slower [$t_{(30)} = 8.47$; $p < 0.001$ (unc.)] when answering perceptual compared with conceptual questions (Fig. 1*d*,*e*). The discrepancy between the EEG and fMRI samples, together with the difference in subjective retrieval time, suggests that participants in the fMRI study often pressed the subjective retrieval button before recall was complete, such that the feature reconstruction process carried over into the catch question period (Linde-Domingo et al., 2019; Lifanov et al., 2021).

Despite these RT differences, accuracies were comparably high in the two samples. Moreover, in the EEG–fMRI fusion analyses reported further below, the fMRI data are mainly used to derive the spatial representational patterns, while the precise time resolution is provided by the EEG data (for a review, see Jorge et al., 2014). Considering the sluggishness of the hemodynamic response (Friston et al., 1994; Kruggel and von Cramon, 1999; Glover, 2011), the faster button presses in the fMRI sample should thus only have minimal effects on the fusion results.

EEG multivariate results

Plots in Extended Data Figure 4-1 show the time-resolved decoding accuracy from the cross-subject classifier, once in gray averaged across all object pairings in the RDM and in magenta split into the pairings belonging to the same (within) or different (between) conceptual classes, all with corresponding statistics (see Materials and Methods).

During encoding, individual object decoding accuracy started increasing gradually from ~25 ms after the stimulus onset, with a first smaller peak ~127 ms [$p < 0.05$ (cluster)] and a second temporally extended cluster from 236 ms until the end of the trial [$p < 0.05$ (cluster)]. Moreover, objects from conceptually different classes (animate vs inanimate) were classified significantly better than objects from the same class, starting from 220 ms after the stimulus onset until 1.3 s [$p < 0.05$ (cluster)]. Given the object recognition literature (Cichy et al., 2014), it was surprising that the accuracy of object-identity decoding was comparatively low (though still significant) within the first 100 ms compared with the time period after 200 ms. This might reflect the fact that across participants, the objects corresponded in terms of image content but not perceptual format, potentially suppressing some low-level similarities and thus making classification on early visual features more difficult. That said, the photographic and drawn object versions overlapped in shape, orientation, and disparity, preserving at least some low-level features, and a classifier should thus be able to use the neural signals corresponding to these features to discriminate individual objects. In fact, the searchlight fusion shows major correlation clusters during encoding in early visual areas (Fig. 5*a*), indicating that some low-level features contribute to decoding performance at these early time points.

During retrieval, overall cross-subject classification accuracies remained relatively low in comparison with encoding, showing a peak decoding accuracy of 51% approximately −2.8 s before the retrieval button press. Five significant accuracy clusters were found with peaks located at times −2.74, −2.63, −2.56, −2.16, and −1.47 s relative to the time of subjective recollection [all $p < 0.05$ (cluster)]. When comparing classification accuracy for conceptually different, between-class object pairs to within-class pairs, this comparison survived cluster correction at no time point. The maximum between- versus within-class difference was identified about −2.5 s before the retrieval button press, though at a very liberal threshold [$p < 0.01$ (unc.)].

fMRI multivariate results

Previous work suggests that during memory recall, conceptual information becomes accessible earlier than perceptual information, as evidenced in neural pattern decodability (Linde-Domingo et al., 2019) and behavior (Lifanov et al., 2021; Linde-Domingo et al., 2019; and in this paper, Fig. 1*d*). The first aim of the present study was to determine the locus of these perceptual and conceptual representations both during encoding and retrieval. We thus performed a searchlight-based LDA. Two separate classifiers were trained to distinguish between the different perceptual (photographs vs drawings) and the different conceptual (animate vs inanimate) classes of our visual objects (see Materials and Methods for details). During encoding (Fig. 2*a*), when the object was present on the screen, perceptual class could be decoded in posterior regions along the ventral visual stream including V1, V2, lingual, and fusiform gyrus [$t_{(30)} = 4.98$; $p < 0.05$ (FWE)]. Conceptual class was decodable from more anterior lateral temporal lobe areas, including inferior, mid, and superior temporal gyrus, and from the precuneus and the inferior frontal gyrus, dorsolateral prefrontal cortex, and anterior prefrontal cortex [$t_{(30)} = 4.82$; $p < 0.05$ (FWE)]. Together, this mapping generally reflects a posterior-to-anterior perceptual-to-conceptual processing gradient. The results largely mirror the univariate analyses (Extended Data Fig. 2-2) and complement them by showing additional content decoding in frontal and parietal regions, suggesting that these areas code information in fine-grained multivoxel patterns that univariate analyses are unable to capture.

During retrieval (Fig. 2*b*), perceptual features were most strongly decodable in the precentral gyrus (i.e., the premotor cortex) but also in the precuneus, angular gyrus, cingulate cortex, inferior frontal gyrus, and ventral areas including V2, fusiform gyrus, and middle temporal lobe [$t_{(30)} = 4.80$; $p < 0.05$ (FWE)]. Conceptual category membership was classified with the highest accuracy from fusiform gyrus, middle temporal gyrus, temporal pole, precuneus, angular gyrus, dorsolateral prefrontal cortex, and inferior and superior frontal gyrus [$t_{(30)} = 4.60$; $p < 0.05$ (FWE); for detailed LDA results, see

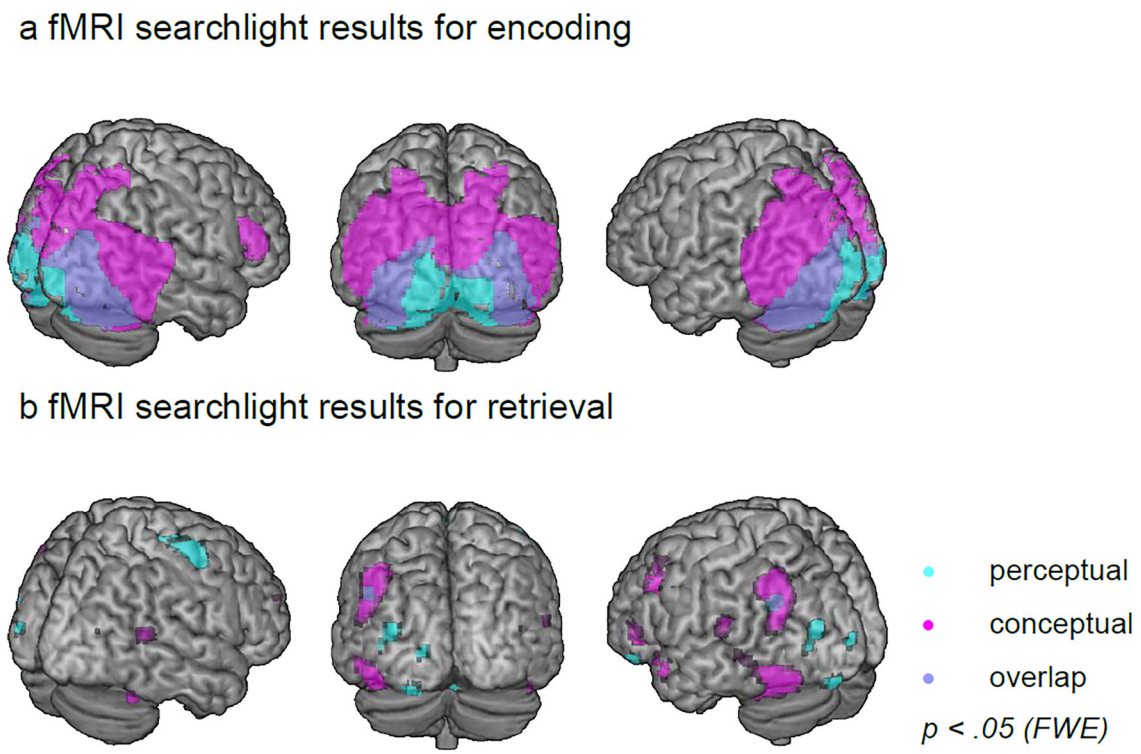

Figure 2. Searchlight LDA results. Second-level *t*-contrasts show (***a***) encoding and (***b***) retrieval accuracies significantly higher than the 50% chance level when classifying perceptual (cyan) and conceptual (magenta) object features; overlap is indicated in purple. All contrasts are thresholded at $p < 0.05$ (FWE-corrected). $N = 31$ independent subjects. Figure made using MRIcron (https://www.nitrc.org/projects/mricron, www.mricro.com, Rorden and Brett, 2000) and a Colin 27 average brain template (http://www.bic.mni.mcgill.ca/ServicesAtlases/Colin27, Holmes et al., 1998; Copyright (C) 1993–2009 Louis Collins, McConnell Brain Imaging Centre, Montreal Neurological Institute, McGill University). See Extended Data Figures 2-1 and 2-2 and Extended Data Tables 2-3–2-9 for more details.

Extended Data Tables 2-3–2-6*b*]. Hence, in addition to the ventral visual areas dominating encoding/perception, we also found extensive frontal and parietal areas in our retrieval searchlight, in line with previous work suggesting that mnemonic as opposed to sensory content can often be decoded from these areas (Kuhl and Chun, 2014; Favila et al., 2018, 2020; Ferreira et al., 2019). At liberal thresholds, a paired *t* test (Extended Data Table 2-6*b*) contrasting perceptual versus conceptual classifications during retrieval showed higher conceptual classifications in the frontal [$t_{(30)} = 3.46$; $p = 0.001$ (unc.)], dorsolateral prefrontal cortex [$t_{(30)} = 3.28$; $p = 0.001$ (unc.)], temporal pole [$t_{(30)} = 2.71$; $p = 0.005$ (unc.)], and precuneus [$t_{(30)} = 2.47$; $p = 0.01$ (unc.)]. Paired *t* tests at the same liberal thresholds showed no higher accuracies for perceptual decoding during retrieval. Together, the fMRI-based classification of the two dimensions that we explicitly manipulated demonstrates that brain activity patterns during the retrieval of object images carry information about perceptual format and conceptual content, with the latter dominating the recall patterns. Some areas partially overlapped with the areas seen at encoding, but retrieval additionally comprised unique contributions in frontoparietal networks (overlap visualized in Extended Data Fig. 2-1). Note, also, that regional overlap in content decodability in this analysis does not necessarily imply and exact pattern overlap between encoding and retrieval.

No voxels survived (at $p < 0.05$, FWE-corrected) when cross-classifying perceptual or conceptual categories from encoding to retrieval or from retrieval to encoding, which might be due to the overall noisier retrieval patterns, or due to a transformation of these category representations between encoding and retrieval (see Discussion).

EEG–fMRI data fusion

EEG multivariate analysis

The next goal of this study was to map the spatial patterns in a given brain area onto the EEG patterns present at each time point of a trial, to reveal how content representations evolve over the time course of encoding and retrieval. For this data fusion, we first needed to obtain a meaningful EEG matrix representing object-to-object similarities for each time point of encoding and retrieval, which we could then compare with the fMRI-based matrices. Correlation-based RDMs for the EEG data were too noisy to see a meaningful match between modalities (see Materials and Methods, Analyses that did not work). We thus created a classification-based matrix representing the dissimilarities between each pair of objects, in each EEG time bin, based on a cross-participant classifier. Amplitudes over the 128 electrodes at a given time point served as classification features, and our 24 participants provided the repetitions of each object. The pairwise

classification accuracies were entered in a single, time-resolved RDM structure representing the dissimilarity between individual objects of our stimulus pool collapsed across participants (Fig. 3*a*). For all fusion analyses, we investigated encoding timelines from the image onset and retrieval timelines leading up to the subjective button press.

ROI fusion

Having obtained this EEG-based similarity time course, we performed a similarity-based fusion of the EEG and fMRI data, probing what brain regions (in the fMRI data) most closely matched the similarity structures contained in the EEG data at any given time point during encoding and retrieval. For a first fusion step, we used the representational geometries

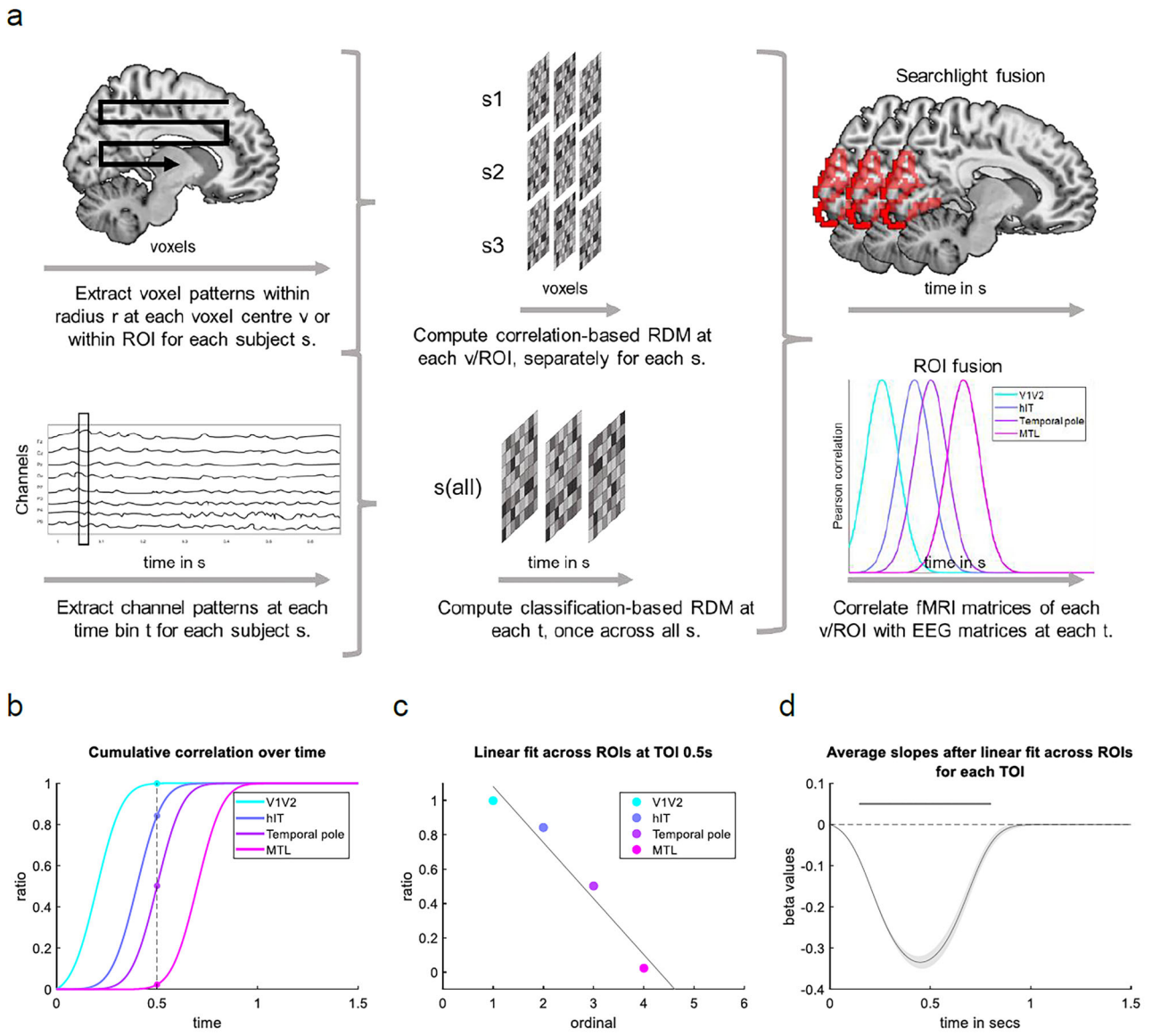

Figure 3. ***a***, Overview of ROI and searchlight fusion. First, brain activity patterns are extracted from fMRI and EEG to create RDMs in the spatial and temporal domain, respectively. Then, second-order correlations of the RDMs from the two imaging modalities are computed for the data fusion. The EEG RDMs are classification-based, derived from binary classifiers trained and tested to distinguish each pair of objects across participants. FMRI RDMs are computed within participants and are correlation-based. FMRI RDMs can be computed at each voxel center (v) including voxels within a specific radius or for larger ROI. Depending on this choice, the data fusion will be searchlight- or ROI-based, respectively. ***b***, ***c***, Linear regression approach on ROI time courses in a forward stream simulation. ***b***, Normalized cumulative sum of each ROI time course of the ventral visual stream. At time point 0.5 s, earlier visual regions show a higher cumulative sum than later regions along the ventral visual stream. ***c***, A linear regression is fitted across ROI values at 0.5 s and results in a negative slope. ***d***, Average slopes and standard errors are illustrated for each time point across the window 0–1.5 s and tested against zero. Significant time points are indicated by points ($p < 0.01$ unc.). Method and panels ***b–d*** adapted from Michelmann et al. (2019). Brain figures made using MRIcron (https://www.nitrc.org/projects/mricron, www.mricro.com, Rorden and Brett, 2000), a Colin 27 average brain template (http://www.bic.mni.mcgill.ca/ServicesAtlases/Colin27, Holmes et al., 1998; Copyright (C) 1993–2009 Louis Collins, McConnell Brain Imaging Centre, Montreal Neurological Institute, McGill University) and WFU PickAtlas v3.0 (Lancaster et al., 1997, 2000; Tzourio-Mazoyer et al., 2002; Maldjian et al., 2003, 2004).

(i.e., the RDMs) from an anatomically predefined set of ROIs. We then calculated the correlation between these ROIs' representational geometries and the geometries obtained from the EEG data for each time bin (Fig. 3*a*) and statistically compared the correlations against zero using cluster-basted permutation testing.

To statistically evaluate whether the information flow is primarily forward or backward along ventral visual stream areas, we used a linear regression on the cumulative sums of the correlation time courses of the corresponding ROIs, a method previously established for MEG analyses (Michelmann et al., 2019). The intuition of this method is that if Region 1 starts accumulating information before Region 2 and Region 2 before Region 3, the cumulative sums will line up sequentially to reflect this systematic delay in information accumulation (Fig. 3*b–d*, simulation). In our case, we expected forward progressing latencies along the ventral visual stream during encoding and backward progressing latencies during retrieval (Fig. 3*b–d*).

Our predefined set of ROIs included regions along the ventral visual stream (V1/V2, hIT, temporal pole, and MTL), and regions along the dorsal stream (superior parietal lobe, lateral inferior parietal cortex, and medial parietal cortex; see Materials and Methods, ROIs). Since many computational models propose that the role of the hippocampus is related to association or indexing rather than feature representation (Teyler and DiScenna, 1986; McClelland et al., 1995; Eichenbaum, 2001; O'Reilly and Norman, 2002; Rolls, 2010, 2013), we excluded the hippocampus from the MTL regions. In Figure 4*a–d*, correlation time courses are plotted for each individual ROI as *t* values resulting from *t* tests against zero, with clusters resulting from a cluster-based permutation test (see Materials and Methods, Analyses). The figure shows ventral visual regions in panel *a*/*c* and dorsal regions in panel *b*/*d*. Note that in-text significance statements give information about uncorrected *p* values (unc.), *p* values Bonferroni's corrected for multiple comparisons (Bonferroni's, 1936), temporal clusters, or temporal clusters additionally corrected for multiple comparisons.

Following the object onset at encoding (Fig. 4*a*), posterior regions including V1 and V2 showed an increasing correlation with the EEG representations from ∼120 ms [$p < 0.01$ (mc corr.)]. A significant cluster was seen from 240 ms onward and remained active for ∼1 s [$p < 0.05$ (corr. cluster)], followed by another cluster at 1.31 s after the image onset [$p < 0.05$ (unc. cluster)]. The first cluster was followed by a correlation increase of later ventral visual areas (the hIT cortex) ∼310 ms, reaching a significant peak at ∼420 ms [$p < 0.05$ (corr. cluster)]. Later lateral and medial temporal as well as parietal regions (Fig. 4*b*) did not show a significant correlation with the EEG time series during encoding.

As a proof of principle, we then tested for a forward processing stream in the encoding data across ventral visual areas. Performing a linear regression on the cumulative sums of all ventral ROI time courses at each time point (see Materials and Methods, Fig. 3*b–d*, Extended Data Fig. 4-2*a*,*c*), we found negative slopes reaching significance 500 ms after the stimulus onset [$p < 0.05$ (cluster)]. This finding statistically corroborates the observation that earlier ventral visual regions code relevant information before later regions, supporting the well established forward stream (Fig. 4*e*). It should be noted, however, that evidence for such feedforward processing was only present relatively late in the trial, likely since the strongest peaks of object-identity decoding also fell in this late time window (Extended Data Fig. 4-1*a*).

When performing the same analysis for ventral visual ROIs during retrieval (Fig. 4*c*), several regions peaked below the threshold of cluster significance: MTL regions showed a peak correlation with the EEG representational geometries −2.96 s [$p < 0.01$ (mc corr.)] and −2.82 and −1.97 s prior to the retrieval button press [$p < 0.01$ (unc.)]. Furthermore, correlation peaks were found for the temporal pole at −2.13 s [$p < 0.01$ (unc.)]. HIT showed a peak correlation with the EEG geometry at −1.33 s [$p < 0.01$ (mc corr.)] and −1.22 s [$p < 0.01$ (unc.)], forming a cluster at −1.27 s [$p < 0.05$ (unc. cluster)]. Similarly, V1/V2 peaked at −1.33 s [$p < 0.01$ (unc.)], showing a cluster at −1.27 s before button press [$p < 0.05$ (unc. cluster)].

Within the dorsal set of ROIs (Fig. 4*d*), the inferior medial parietal lobe showed a correlation peak in a similar time window, at −1.33 s before button press [$p < 0.05$ (unc. cluster)]. This and the peak of the inferior lateral parietal ROI at −1.22 s [$p < 0.01$ (unc.)], as well as superior parietal ROI at −1.25 s [$p < 0.01$ (unc.)], coincided with the peak times of posterior ventral visual areas (V1/V2/hIT).

Our main aim of the data fusion was to test if memory reactivation followed a backward processing hierarchy along the ventral visual stream. We therefore also performed a linear regression on cumulative sums of ventral visual regions within retrieval (Extended Data Fig. 4-2*b*,*d*). This analysis revealed a significant positive slope from −2.2 to −1.3 s before button press [$p < 0.05$ (cluster)], speaking in favor of a backward stream and thus confirming our main hypothesis (Fig. 4*f*).

Searchlight fusion

Next, in a more explorative but also spatially better resolved approach, we conducted a whole-brain searchlight fusion to inspect where across the brain the fMRI-based representational geometries matched the EEG geometries over time. Figure 5 depicts spatial *t*-maps representing significant EEG–fMRI correlations in each searchlight radius for a given time bin, separately at encoding (Fig. 5*a*) and retrieval (Fig. 5*b*). The maps only show time points where significant spatial clusters emerged. During encoding, the searchlight fusion revealed a significant cluster in V1 and lingual gyrus at 60 ms following the object onset and again from 130 to 160 ms and from 240 ms onward, reactivating several more times (e.g., see timepoints 940 ms and 1.3 s) before fading ∼1.4 s after the stimulus onset. Importantly, over the time course of object perception, significant clusters of EEG–fMRI similarity gradually extended from early visual (V1, V2) to more ventral and lateral areas, including fusiform and inferior temporal gyrus. For the encoding data, the results of the searchlight approach

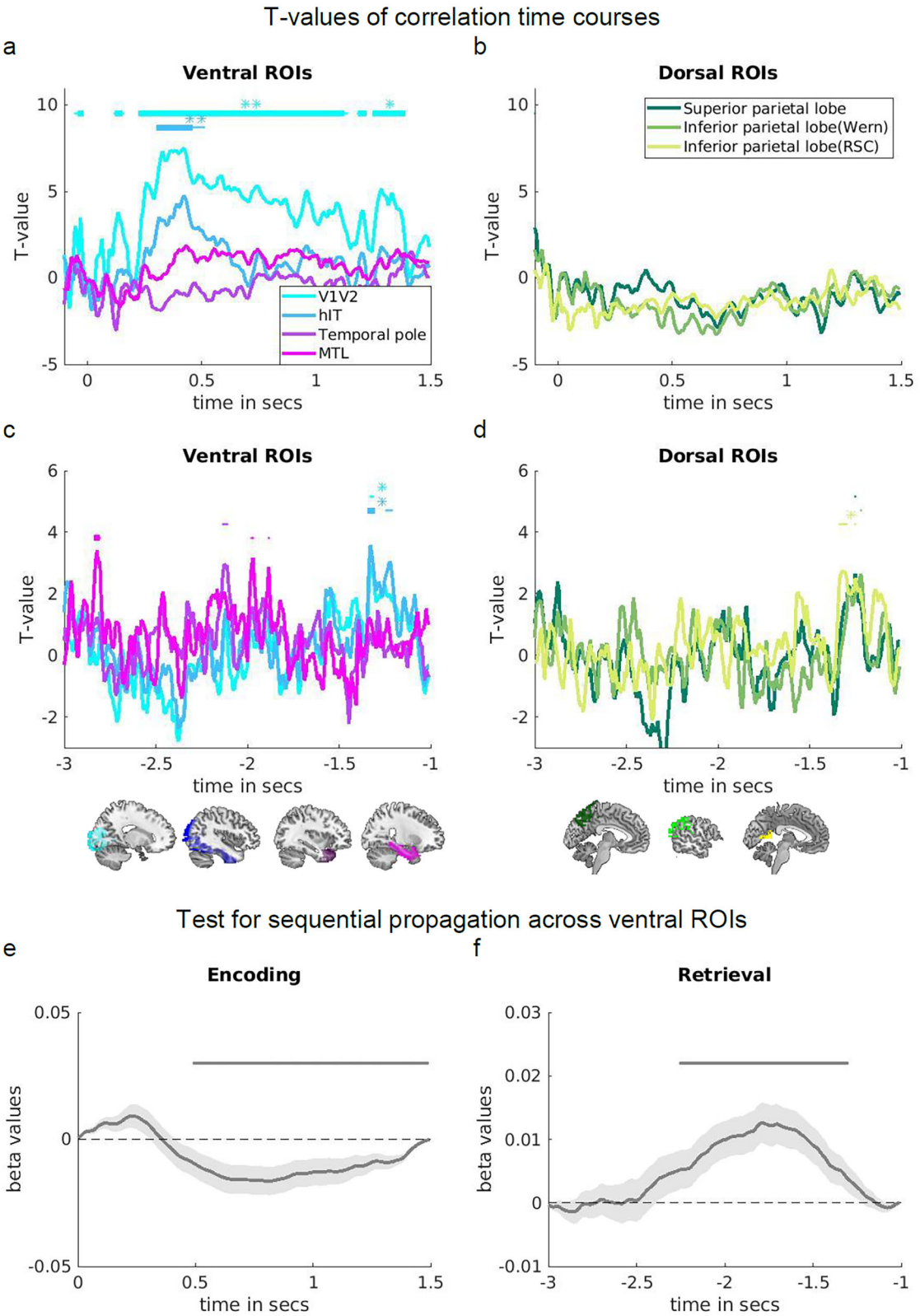

Figure 4. ***a–d***, *T* values from one-sample *t* test of correlation time courses between the EEG RDMs and ventral visual (***a***, ***c***) and dorsal (***b***, ***d***) ROIs during encoding (***a***, ***b***) and retrieval (***c***, ***d***). ROIs are color-coded as indicated in the legends. Significant time points are indicated by points ($p < 0.01$ uncorrected), squares ($p < 0.01$ Bonferroni corrected for multiple comparison of 7 ROIs), one asterisk ($p < 0.05$ cluster), and two asterisks ($p < 0.05$ cluster, Bonferroni corrected for multiple comparison of 7 ROIs). ***e***, ***f***, Results of the test for sequential processing, using a linear fit of the cumulative sums of correlation time courses across ROIs within the ventral visual stream at (***e***) encoding and (***f***) retrieval. Average slopes and standard errors are shown for each time

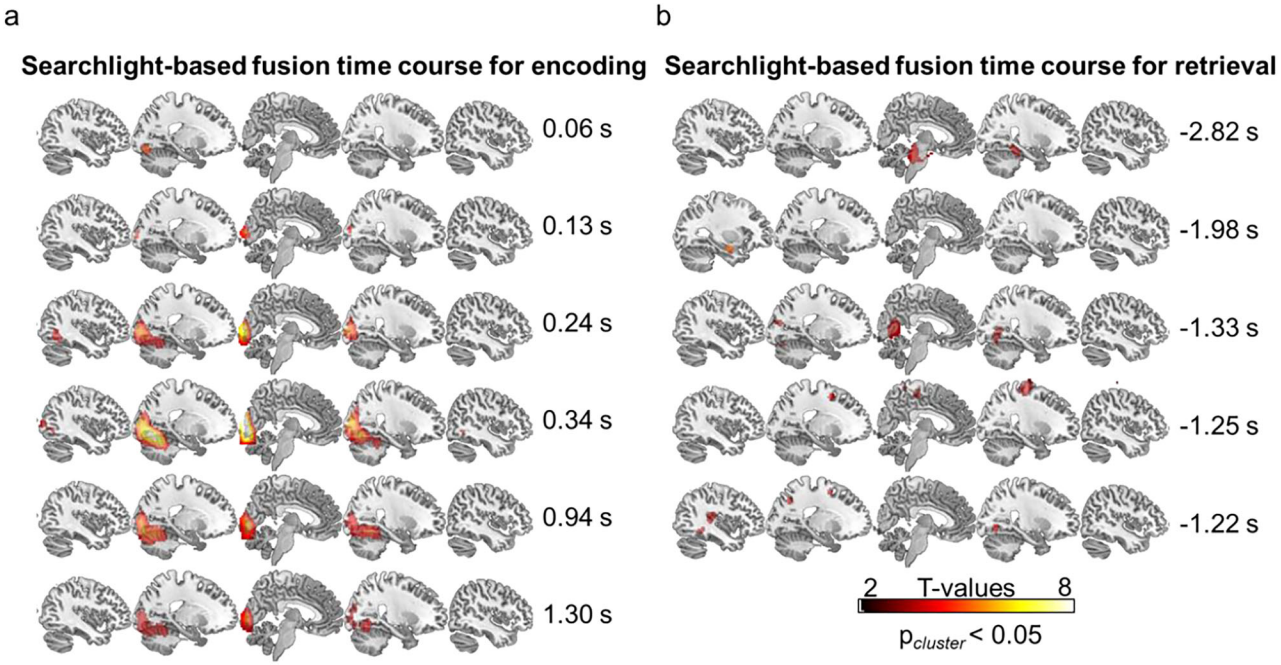

Figure 5. *T*-maps from one-sample *t* test of EEG–fMRI correlations at (***a***) encoding and (***b***) retrieval showing time points in the trial time course where significant spatial clusters of correlations emerged ($p_{cluster} < 0.05$; see Materials and Methods for further details). *T* test involved a spatial maximal permuted statistic correction combined with a threshold-free cluster enhancement (Nichols and Holmes, 2002; Smith and Nichols, 2009). At encoding, time point 0 s would mark the object onset. At retrieval, time point 0 s marks the button press; however, both zero time points are not included in figure as no clusters emerged. $N = 31$ independent subjects. Brain figures made using MRIcron (https://www.nitrc.org/projects/mricron, www.mricro.com, Rorden and Brett, 2000) and a Colin 27 average brain template (http://www.bic.mni.mcgill.ca/ServicesAtlases/Colin27, Holmes et al., 1998; Copyright (C) 1993–2009 Louis Collins, McConnell Brain Imaging Centre, Montreal Neurological Institute, McGill University).

thus overlap with the ROI fusion results and mainly reveal ventral visual stream activation progressing in a forward (early-to-late visual cortex) manner.

During retrieval, the earliest cluster of significant EEG–fMRI correlations was found in the fusiform area, preceding the subjective retrieval button press by −2.82 s, accompanied by a small cluster in the pons. Contrary to our prediction, we also observed pattern overlap in the hippocampus at −1.98 s before button press.

At time points closer to the button press, additionally clusters showing significant pattern correlations were found in lower-level regions. At −1.33 s, V1, V2, V4d, and the fusiform gyrus showed significant clusters. Furthermore, at −1.25 s, clusters were found in the premotor cortex, primary motor cortex, and superior parietal lobule (SPL). Finally, clusters were found in the premotor cortex, SPL, primary and associative visual cortex, fusiform area, and Wernicke's area at −1.22 s before subjective retrieval.

Together, the retrieval data showed convergence between the ROI and searchlight fusion approach. It showed a progression of the peak correlations from frontotemporal to posterior sensory and parietal regions, generally reflecting a backward propagating processing stream which, however, only partially revisits the areas involved during encoding, thus suggestive of substantial transformations between object perception and memory reconstruction.

Discussion

What mnemonic content is recovered, where in the brain during memory retrieval, and how does the hippocampal–neocortical pattern completion process unfold in time? Recent memory research suggests that the information processing

←

point and statistically tested against zero. A negative slope suggests that earlier ROIs along the ventral visual stream have a higher cumulative sum than later ROIs, indicative of a forward stream. According to the same logic, a positive slope indicates a backward stream. Significant time points are indicated by gray points above the curve ($p < 0.05$ cluster). Method adapted from Michelmann et al. (2019). In all subpanels, time point 0 s marks the object onset during encoding and the subjective recall button press during retrieval. The latter is not included on time axis as it does not lie within the time window of interest (see Materials and Methods also for details on cluster correction). Variance in all subpanels comes from $n = 31$ independent subjects. Brain figures made using MRIcron (https://www.nitrc.org/projects/mricron, www.mricro.com, Rorden and Brett, 2000), a Colin 27 average brain template (http://www.bic.mni.mcgill.ca/ServicesAtlases/Colin27, Holmes et al., 1998; Copyright (C) 1993–2009 Louis Collins, McConnell Brain Imaging Centre, Montreal Neurological Institute, McGill University), and WFU PickAtlas v3.0 (Lancaster et al., 1997, 2000; Tzourio-Mazoyer et al., 2002; Maldjian et al., 2003, 2004). See Extended Data Figures 4-1 and 4-2 for more details.

hierarchy is reversed during the recall of a visual object from episodic memory compared with its initial perception (Linde-Domingo et al., 2019; Lifanov et al., 2021; Mirjalili et al., 2021), with conceptual features becoming available earlier than perceptual features. Here, we investigated the locus of these feature representations during encoding and recall using fMRI-based decoding. Additionally, EEG–fMRI fusion allowed us to test whether this presumed reversed information processing cascade during memory reconstruction maps onto the same ventral visual stream areas that carry the information forward during perception but now following a backward trajectory. Our study shows that recall is largely dominated by conceptual information in the posterior ventral regions and that the reconstruction of visual object memories, while following a backward trajectory along ventral visual object processing pathways to some extent, also involves an information relay to parietal and frontal regions.

We first used uni- and multivariate analyses on the fMRI data alone to map out the regions processing perceptual and conceptual object dimensions that were built into the stimulus set. As expected, during encoding when the object was visible on the screen, these features largely mapped onto the ventral visual pathway, where early visual areas coded the perceptual features (colored photos vs black-and-white line drawings), whereas later visual areas coded the mid- to higher-level conceptual information (animate vs inanimate objects; B. Long et al., 2018). This general perceptual-to-conceptual gradient is in line with a multitude of findings in the basic object recognition and vision literature (Carlson et al., 2013; Kravitz et al., 2013; Cichy et al., 2014).

Univariate analyses were not powerful enough to detect differential activations between perceptual and conceptual categories when objects were reconstructed from memory. Activity patterns at the finer-grained multivoxel level, however, carried information about the categorical features of the retrieved images. Memory-related reactivation of these features comprised some regions also found during object encoding, particularly in late visual areas (Fig. 2*b*, Extended Data Fig. 2-1). This partial overlap confirms a body of previous work showing that posterior visual areas are not only involved in visual perception but also in internally generated processes, such as mental imagery (Kosslyn et al., 1993; Dijkstra et al., 2021) or episodic memory. While most memory studies find reactivation in late areas along the ventral stream (Polyn et al., 2005; Staresina et al., 2012; Griffiths et al., 2019), others have reported areas as early as V1 (Bosch et al., 2014). It is also commonly observed that stronger reinstatement is associated with memory success and strength (Huijbers et al., 2011; Staresina et al., 2012; Ritchey et al., 2013; Wing et al., 2014; Thakral et al., 2015) and the vividness and detail of remembering (Wheeler et al., 2000; St-Laurent et al., 2015; Bone et al., 2020; Simons et al., 2022), suggesting an important functional role of sensory reactivation. Assuming a hierarchical reverse processing from higher to lower sensory regions during recall, incomplete retrieval would lead primarily to a loss of perceptual information. Premature retrieval button presses, as found in the present study (see behavioral results), could indicate such incomplete recall and explain the overall weaker decodability of perceptual features.

Although the spatial localizations of feature-specific patterns during recall partly overlapped with those found during encoding, they also encompassed regions outside the ventral visual object processing pathways. Most notably, conceptual object information during recall was decodable from frontal and parietal regions. The role of the frontoparietal cortex in representing mnemonic information is still debated (Buckner et al., 1999; Kramer et al., 2005; Levy, 2012; Favila et al., 2018, 2020; Staresina and Wimber, 2019; Humphreys et al., 2021; Xue, 2022). Some studies suggest that depending on the task and functional state (i.e., encoding or retrieval), content representations are preferentially expressed in sensory or parietal cortices, respectively, and mediated by differential connectivity with the hippocampus (Favila et al., 2018; N. M. Long and Kuhl, 2021; for a related review about the posterior medial network, see Ritchey and Cooper, 2020). Others propose that parietal areas provide a contextualization of the retrieved memories (Jonker et al., 2018). Our findings support the previously described encoding–retrieval distinction and suggest that it is predominantly conceptual information (Fig. 2*b*, Extended Data Table 2-6*b*) that is represented in parietal regions during retrieval, in line with previous work showing strong object identity—and even abstract concept coding in the parietal cortex (Jeong and Xu, 2016; Ferreira et al., 2019; Kaiser et al., 2022). The involvement of parietal networks is also discussed further below in relation to the timing of the reactivation.

Going beyond a purely spatial mapping of perceptual and conceptual representations, fusing the EEG and fMRI data allowed us to inject time information into these spatial maps and to ask how the memory reconstruction stream evolves, building up to the time of subjective recollection. We used two complementary approaches for data fusion, both comparing the representational geometries found in the EEG patterns at each time point with the fMRI geometries found in a given brain region. Both the ROI-based and searchlight-based approach showed a mainly feedforward sweep of information processing during the first few hundred milliseconds of object perception, starting within early visual regions ~60 (searchlight fusion) to 120 ms (ROI fusion) after the image onset and spreading to more ventral visual regions within the next 200 ms (see Materials and Methods, Searchlight fusion and ROI fusion). Interestingly, we observed a sustained response in early visual regions, which we believe to partially be a consequence of the task demand that included visualizing the object for encoding purposes. Importantly, a formal regression analysis allowed us to statistically corroborate the spatiotemporal direction of information flow, by modeling the information accumulation rate across the hierarchy of ventral visual stream regions (Michelmann et al., 2019). Note that while this regression is a powerful method for detecting serial processes across participants (Michelmann et al., 2019), it merely speaks to the order of patterns seen in the ROI time courses, irrespective of the strength and significance of these ROIs' average peaks. The method should thus be regarded as complementing the ROI-based and searchlight-based fusion analyses. During encoding, later ROI peaks did not show

significant correlations, likely due to less time-locked nature of late EEG peak, leading to comparatively smaller mapping effects in the fusion (for comparison, see Cichy et al., 2014, 2016). That said, the results statistically support a posterior-to-anterior progression of the correlation patterns across participants during early phases of the encoding trials, likely driven disproportionally by V1/V2 and hIT patterns.

Similarly, the EEG–fMRI fusion and sequence analyses were applied to the retrieval data. We acknowledge that the retrieval EEG–fMRI correlations were comparatively weak and would, in the case of the fusion analysis, not survive an additional correction for multiple comparisons over time on top of the spatial cluster-based correction. That said, the temporal evolution of effects still offer insights into the memory reconstruction process. The ROI data fusion and linear regression hint at a largely backward information processing trajectory, with information flowing from MTL (both fusion approaches) and temporal pole (ROI fusion) to more posterior visual regions (both fusion approaches). The temporal pole has previously been associated with processing of high-level semantic information (Noppeney and Price, 2002; Patterson et al., 2007; Visser et al., 2010; Rice et al., 2018; Clarke, 2020). Moreover, temporal pole reactivation around −2.1 s before button press was close to the time point when objects from different conceptual classes were more discriminable than objects from similar conceptual classes based on the EEG classification alone (Extended Data Fig. 4-1*b*). Note that our decoding peaks were found considerably earlier than in previous work (Linde-Domingo et al., 2019), likely due to the cross-participant object–identity decoding approach (for comparison, see Linde-Domingo et al., 2019; Mirjalili et al., 2021) which may rely on higher-level exemplar–level information presumably processed close to the hippocampus (Clarke and Tyler, 2015). Together with our previous work using feature-specific reaction times (Linde-Domingo et al., 2019; Lifanov et al., 2021), these findings indicate that conceptual object features in semantic networks are among the first to be reactivated during memory retrieval, which might be indicative of a semanticization process introduced by retrieval (Lifanov et al., 2021).

More posterior areas including inferior temporal, inferior parietal, and visual cortices, as well as frontal regions, reached their representational correlation peaks considerably later, from −1.33 s before button press onward (Figs. 4*c*,*d*, 5*b*). While visual activations can be assumed to represent the perceptual content of the reactivated memories, the role of fronto-/parietal regions, as mentioned earlier, is still a matter of debate (Naghavi and Nyberg, 2005; Barry and Maguire, 2019; Fischer et al., 2021). In addition to the potential semanticization process discussed in the previous paragraph, parietal areas have been shown to play a role in contextual processing, imagery during recall, and scene construction (Fletcher et al., 1995; Lundstrom et al., 2005; Chrastil, 2018). The latest reactivations might thus be indicative of a final stage of recall leading up to subjective recollection, likely involving working memory and memory-related imagery and, hence, preparation for the upcoming categorization task (Ganis et al., 2004; Christophel et al., 2012, 2017). In summary, contrary to encoding, we find that retrieval follows a backward propagation along the ventral visual stream. Moreover, the backward reconstruction flow is not limited to ventral visual brain areas that dominate the encoding patterns but instead involves frontal and parietal regions that may serve as an episodic memory or imagery buffer for the retrieved representations (Baddeley, 1998, 2000; Wagner et al., 2005; Levy, 2012), speaking in favor of a transformative process.

The anterior-to-posterior retrieval stream shown here is reminiscent of a similar reversed stream for object imagery in the absence of an episodic cue (Dijkstra et al., 2020), which has also been described as progressing in a hierarchical fashion along the ventral stream (Horikawa and Kamitani, 2017). Generating mental images from general knowledge compared with cuing them from episodic memory likely involve different neural sources, in the latter case most notably the hippocampus. However, both processes rely on the internal generation of stored mental representations (i.e., memories), and it is thus perhaps not surprising that mental imagery and episodic retrieval overlap in many aspects, including their reverse reconstruction gradient. While there have been various studies comparing imagery with perception (Horikawa and Kamitani, 2017; Dijkstra et al., 2020; Xie et al., 2020), it will be interesting for future studies to provide a more detailed picture of where in the processing hierarchy imagery and memory retrieval overlap.

The fMRI classification and the RSA-based EEG–fMRI fusion in this study offer complementary information. RSA is a useful tool to enable the comparison of neural representations measured by different neuroimaging modalities (Kriegeskorte and Kievit, 2013). By creating similarity structures from EEG and fMRI activity patterns in the same format, it becomes possible to directly correlate the representational geometries emerging in neural space and time. However, the RSA-based data fusion is in itself blind to the informational content that is driving the match in representations (Schyns et al., 2020). Classification-based approaches on fMRI (or EEG) data, on the other hand, can pinpoint categorical representations that are explicitly built into the experimental design. However, they are restricted to very few categories (e.g., animacy, color), in turn limiting the conclusions that can be drawn about the certainly much richer and more multidimensional content of mental (memory) representations. In sum, data fusion and categorical decoding methods offer complementary insights into the content of reactivated memories, likely explaining why, in our study, some correlation peaks in the searchlight fusion maps during retrieval did not overlap with the sources of either perceptual or conceptual features. Richer study designs with more stimulus variations on a trial-by-trial basis (Schyns et al., 2020) are a promising avenue for revealing what type of content representations are contained in, and dominate, reactivated memories. An exciting recent development is the use of deep neural networks (DNNs) trained on image categorization and to compare the networks' layer patterns with the representational patterns that emerge in the real brain (Cichy et al., 2019; E. J. Allen et al., 2022). Some recent work has employed this approach to shed light onto the nature of reactivated memory representations, for example, to investigate what level of feature reactivation predicts the vividness and distinctiveness of a

memory (Bone et al., 2020). Others have used DNNs in comparison with intracranial EEG to reveal memory transformations over time and across different processing stages (Liu et al., 2020). Finally, different types of models, including word embedding models, have been used to uncover the temporal and content structure of recall narratives and how it compares with the original encoding (Heusser et al., 2021). In contrast to the relative black box of DNN layers, the latter models offer more transparency and interpretability of the dimensions contained in a memory and a route to understanding how the recall of naturalistic, continuous events unfolds in time.

In summary, our EEG–fMRI data fusion supports the idea of a retrieval process that at least partially progresses in reverse along the ventral visual stream with respect to encoding. Relating these findings to the fMRI decoding, which indicate a dominance of conceptual representations in later ventral regions and some perceptual representations in lower-level areas, it is likely to assume a conceptual-to-perceptual processing gradient during memory retrieval. Additionally, we show that the backward trajectory of memory reconstruction is not limited to ventral visual stream regions involved during encoding but also engages multisensory frontoparietal areas at distinct stages of retrieval processing, in line with the notion of a representational format transformation between perception and memory. The present findings demonstrate how the fusion of temporally and spatially resolved methods can further our understanding of memory retrieval as a staged feature reconstruction process, tracking how the reconstruction of a memory trace unfolds in time and space.

Data Availability

The EEG data acquired by Linde-Domingo et al. (2019) can be found under https://doi.org/10.17605/OSF.IO/327EK. fMRI data can only partly be made publicly available to guarantee full anonymity in accordance with participants' consent. Group-level data and nonidentifiable individual-level data can be found on the Open Science Framework with the identifier https://doi.org/10.17605/OSF.IO/2T7SN. Consent for the reuse of data does not include commercial research. The custom code used in this study is available on the Open Science Framework with the identifier https://doi.org/10.17605/OSF.IO/2T7SN. Additional code associated with the EEG data by Linde-Domingo et al. (2019) can be found under https://doi.org/10.17605/OSF.IO/327EK.

References

Allen EJ, et al. (2022) A massive 7T fMRI dataset to bridge cognitive neuroscience and artificial intelligence. Nat Neurosci 25:116–126.

Allen M, Poggiali D, Whitaker K, Marshall TR, van Langen J, Judd N, Kievit R (2018) RainCloudPlots [Computer software]. RainCloudPlots. Available at: https://github.com/RainCloudPlots/RainCloudPlots

Allen M, Poggiali D, Whitaker K, Marshall TR, van Langen J, Kievit RA (2021) Raincloud plots: a multi-platform tool for robust data visualization. Wellcome Open Res 4:63.

Baddeley A (1998) Recent developments in working memory. Curr Opin Neurobiol 8:234–238.

Baddeley A (2000) The episodic buffer: a new component of working memory? Trends Cogn Sci 4:417–423.

Barry DN, Maguire EA (2019) Remote memory and the hippocampus: a constructive critique. Trends Cogn Sci 23:128–142.

Bone MB, Ahmad F, Buchsbaum BR (2020) Feature-specific neural reactivation during episodic memory. Nat Commun 11:1945.

Bonferroni CE (1936) Teoria statistica delle classi e calcolo delle probabilità. Pubblicazioni del R Istituto Superiore di Scienze Economiche e Commerciali di Firenze 8, 3–62.

Bosch SE, Jehee JFM, Fernández G, Doeller CF (2014) Reinstatement of associative memories in early visual cortex is signaled by the hippocampus. J Neurosci 34:7493–7500.

Brainard DH (1997) The psychophysics toolbox. Spat Vis 10:433–436.

Brodeur MB, Dionne-Dostie E, Montreuil T, Lepage M (2010) The bank of standardized stimuli (BOSS), a new set of 480 normative photos of objects to be used as visual stimuli in cognitive research. PLoS One 5:e10773.

Brodeur MB, Guérard K, Bouras M (2014) Bank of standardized stimuli (BOSS) phase II: 930 new normative photos. PLoS One 9:e106953.

Brodmann K (1909) *Vergleichende Lokalisationslehre der Grosshirnrinde in ihren Prinzipien dargestellt auf Grund des Zellenbaues von Dr. K. Brodmann*. Leipzig: Verlag von Johann Ambrosius Barth.

Buckner RL, Kelley WM, Petersen SE (1999) Frontal cortex contributes to human memory formation. Nat Neurosci 2:311–314.

Carlson T, Tovar DA, Alink A, Kriegeskorte N (2013) Representational dynamics of object vision: the first 1000ms. J Vis 13:1.

Chang C, Glover GH (2010) Time–frequency dynamics of resting-state brain connectivity measured with fMRI. Neuroimage 50:81–98.

Chrastil ER (2018) Heterogeneity in human retrosplenial cortex: a review of function and connectivity. Behav Neurosci 132:317–338.

Christophel TB, Hebart MN, Haynes J-D (2012) Decoding the contents of visual short-term memory from human visual and parietal cortex. J Neurosci 32:12983–12989.

Christophel TB, Klink PC, Spitzer B, Roelfsema PR, Haynes J-D (2017) The distributed nature of working memory. Trends Cogn Sci 21:111–124.

Chrobak JJ, Lrincz A, Buzski G (2000) Physiological patterns in the hippocampo-entorhinal cortex system. Hippocampus 10:457–465.

Cichy RM, Kriegeskorte N, Jozwik KM, van den Bosch JJF, Charest I (2017) Neural dynamics of real-world object vision that guide behaviour. bioRxiv, 147298.

Cichy RM, Kriegeskorte N, Jozwik KM, van den Bosch JJF, Charest I (2019) The spatiotemporal neural dynamics underlying perceived similarity for real-world objects. Neuroimage 194:12–24.

Cichy RM, Oliva A (2020) A M/EEG-fMRI fusion primer: resolving human brain responses in space and time. Neuron 107:772–781.

Cichy RM, Pantazis D (2017) Multivariate pattern analysis of MEG and EEG: a comparison of representational structure in time and space. Neuroimage 158:441–454.

Cichy RM, Pantazis D, Oliva A (2014) Resolving human object recognition in space and time. Nat Neurosci 17:455–462.

Cichy RM, Pantazis D, Oliva A (2016) Similarity-based fusion of MEG and fMRI reveals spatio-temporal dynamics in human cortex during visual object recognition. Cereb Cortex 26:3563–3579.

Clarke A (2020) Dynamic activity patterns in the anterior temporal lobe represents object semantics. Cogn Neurosci 11:111–121.

Clarke A, Taylor KI, Devereux B, Randall B, Tyler LK (2013) From perception to conception: how meaningful objects are processed over time. Cereb Cortex 23:187–197.

Clarke A, Tyler LK (2015) Understanding what we see: how we derive meaning from vision. Trends Cogn Sci 19:677–687.

Dalton MA, D'Souza A, Lv J, Calamante F (2022) New insights into anatomical connectivity along the anterior–posterior axis of the human hippocampus using in vivo quantitative fibre tracking. Elife 11: e76143.
Danker JF, Anderson JR (2010) The ghosts of brain states past: remembering reactivates the brain regions engaged during encoding. Psychol Bull 136:87–102.
Danker JF, Tompary A, Davachi L (2017) Trial-by-trial hippocampal encoding activation predicts the fidelity of cortical reinstatement during subsequent retrieval. Cereb Cortex 27:3515–3524.
Dijkstra N, Ambrogioni L, Vidaurre D, van Gerven M (2020) Neural dynamics of perceptual inference and its reversal during imagery. Elife 9:e53588.
Dijkstra N, van Gaal S, Geerligs L, Bosch S, van Gerven M (2021) No overlap between unconscious and imagined representations. PsyArXiv.
Dobs K, Isik L, Pantazis D, Kanwisher N (2019) How face perception unfolds over time. Nat Commun 10:1258.
Eichenbaum H (2001) The hippocampus and declarative memory: cognitive mechanisms and neural codes. Behav Brain Res 127:199–207.
Favila SE, Lee H, Kuhl BA (2020) Transforming the concept of memory reactivation. Trends Neurosci 43:939–950.
Favila SE, Samide R, Sweigart SC, Kuhl BA (2018) Parietal representations of stimulus features are amplified during memory retrieval and flexibly aligned with top-down goals. J Neurosci 38:7809–7821.
Felleman DJ, Essen DCV (1991) Distributed hierarchical processing in the primate cerebral cortex. Cereb Cortex 1:1–47.
Fellner M-C, Volberg G, Mullinger KJ, Goldhacker M, Wimber M, Greenlee MW, Hanslmayr S (2016) Spurious correlations in simultaneous EEG-fMRI driven by in-scanner movement. Neuroimage 133:354–366.
Ferreira CS, Charest I, Wimber M (2019) Retrieval aids the creation of a generalised memory trace and strengthens episode-unique information. Neuroimage 201:115996.
Fischer M, Moscovitch M, Alain C (2021) A systematic review and meta-analysis of memory-guided attention: frontal and parietal activation suggests involvement of fronto-parietal networks. Wiley Interdiscip Rev Cogn Sci 12:e1546.
Fletcher PC, Frith CD, Baker SC, Shallice T, Frackowiak RSJ, Dolan RJ (1995) The mind's eye—precuneus activation in memory-related imagery. Neuroimage 2:195–200.
Friston KJ, Jezzard P, Turner R (1994) Analysis of functional MRI time-series. Hum Brain Mapp 1:153–171.
Ganis G, Thompson WL, Kosslyn SM (2004) Brain areas underlying visual mental imagery and visual perception: an fMRI study. Brain Res Cogn Brain Res 20:226–241.
Gerber EM (2019) Permutest (version 1.0.0) [Computer software]. MATLAB central file exchange. Available at: https://www.mathworks.com/matlabcentral/fileexchange/71737-permutest (Retrieved February 16, 2021)
Glover GH (2011) Overview of functional magnetic resonance imaging. Neurosurg Clin N Am 22:133–139.
Griffiths BJ, Mayhew SD, Mullinger KJ, Jorge J, Charest I, Wimber M, Hanslmayr S (2019) Alpha/beta power decreases track the fidelity of stimulus-specific information. Elife 8:49562.
Halai AD, Parkes LM, Welbourne SR (2015) Dual-echo fMRI can detect activations in inferior temporal lobe during intelligible speech comprehension. Neuroimage 122:214–221.
Halai AD, Welbourne SR, Embleton K, Parkes LM (2014) A comparison of dual gradient-echo and spin-echo fMRI of the inferior temporal lobe. Hum Brain Mapp 35:4118–4128.
Harris CR, et al. (2020) Array programming with NumPy. Nature 585:357–362.
Heusser AC, Fitzpatrick PC, Manning JR (2021) Geometric models reveal behavioural and neural signatures of transforming experiences into memories. Nat Hum Behav 5:905–919.
Holmes CJ, Hoge R, Collins L, Woods R, Toga AW, Evans AC (1998) Enhancement of MR images using registration for signal averaging. J Comput Assist Tomogr 22:324–333.
Horikawa T, Kamitani Y (2017) Generic decoding of seen and imagined objects using hierarchical visual features. Nat Commun 8:15037.
Huijbers W, Pennartz CMA, Rubin DC, Daselaar SM (2011) Imagery and retrieval of auditory and visual information: neural correlates of successful and unsuccessful performance. Neuropsychologia 49:1730–1740.
Humphreys GF, Lambon Ralph MA, Simons JS (2021) A unifying account of angular gyrus contributions to episodic and semantic cognition. Trends Neurosci 44:452–463.
Inkscape Project (2020) Inkscape (version 1.0.1) [Computer software]. Available at: https://inkscape.org
Insausti R, Muñoz M (2001) Cortical projections of the non-entorhinal hippocampal formation in the cynomolgus monkey (Macaca fascicularis). Eur J Neurosci 14:435–451.
Jeong SK, Xu Y (2016) Behaviorally relevant abstract object identity representation in the human parietal cortex. J Neurosci 36:1607–1619.
Jiang J, Wang S-F, Guo W, Fernandez C, Wagner AD (2020) Prefrontal reinstatement of contextual task demand is predicted by separable hippocampal patterns. Nat Commun 11:2053.
Jonker TR, Dimsdale-Zucker H, Ritchey M, Clarke A, Ranganath C (2018) Neural reactivation in parietal cortex enhances memory for episodically linked information. Proc Natl Acad Sci U S A 115:11084–11089.
Jorge J, Van Der Zwaag W, Figueiredo P (2014) EEG–fMRI integration for the study of human brain function. Neuroimage 102:24–34.
Kaiser D, Jacobs AM, Cichy RM (2022) Modelling brain representations of abstract concepts. PLoS Comput Biol 18:e1009837.
Kirilina E, Lutti A, Poser BA, Blankenburg F, Weiskopf N (2016) The quest for the best: the impact of different EPI sequences on the sensitivity of random effect fMRI group analyses. Neuroimage 126:49–59.
Kleiner M, Brainard D, Pelli D, Ingling A, Murray R, Broussard C (2007) What's new in psychtoolbox-3. Perception 36:1–16.
Kolb H, Fernandez E, Nelson R (1995) Webvision: the organization of the retina and visual system. University of Utah Health Sciences Center. Available at: http://www.ncbi.nlm.nih.gov/books/NBK11530/
Kosslyn SM, Alpert NM, Thompson WL, Maljkovic V, Weise SB, Chabris CF, Hamilton SE, Rauch SL, Buonanno FS (1993) Visual mental imagery activates topographically organized visual cortex: PET investigations. J Cogn Neurosci 5:263–287.
Kramer JH, Rosen HJ, Du A-T, Schuff N, Hollnagel C, Weiner MW, Miller BL, Delis DC (2005) Dissociations in hippocampal and frontal contributions to episodic memory performance. Neuropsychology 19:799–805.
Kravitz DJ, Saleem KS, Baker CI, Ungerleider LG, Mishkin M (2013) The ventral visual pathway: an expanded neural framework for the processing of object quality. Trends Cogn Sci 17:26–49.
Kriegeskorte N (2009) Relating population-code representations between man, monkey, and computational models. Front Neurosci 3:363–373.
Kriegeskorte N, Goebel R, Bandettini P (2006) Information-based functional brain mapping. Proc Natl Acad Sci U S A 103:3863–3868.
Kriegeskorte N, Kievit RA (2013) Representational geometry: integrating cognition, computation, and the brain. Trends Cogn Sci 17:401–412.
Kriegeskorte N, Mur M, Bandettini PA (2008) Representational similarity analysis—connecting the branches of systems neuroscience. Front Syst Neurosci 2:4.
Kruggel F, von Cramon DY (1999) Temporal properties of the hemodynamic response in functional MRI. Hum Brain Mapp 8:259–271.
Kuhl BA, Chun MM (2014) Successful remembering elicits event-specific activity patterns in lateral parietal cortex. J Neurosci 34:8051–8060.
Lancaster JL, Summerlin JL, Rainey L, Freitas CS, Fox PT (1997) The Talairach Daemon a database server for Talairach atlas labels. Neuroimage 5:S633.
Lancaster JL, Woldorff MG, Parsons LM, Liotti M, Freitas CS, Rainey L, Kochunov PV, Nickerson D, Mikiten SA, Fox PT (2000) Automated

Talairach atlas labels for functional brain mapping. Hum Brain Mapp 10:120–131.
Leonardelli E, Fairhall SL (2022) Similarity-based fMRI-MEG fusion reveals hierarchical organisation within the brain's semantic system. Neuroimage 259:119405.
Levy DA (2012) Towards an understanding of parietal mnemonic processes: some conceptual guideposts. Front Integr Neurosci 6:41.
Lifanov J, Linde-Domingo J, Wimber M (2021) Feature-specific reaction times reveal a semanticisation of memories over time and with repeated remembering. Nat Commun 12:3177.
Linde-Domingo J, Treder MS, Kerrén C, Wimber M (2019) Evidence that neural information flow is reversed between object perception and object reconstruction from memory. Nat Commun 10:179.
Liu J, et al. (2020) Stable maintenance of multiple representational formats in human visual short-term memory. Proc Natl Acad Sci U S A 117:32329–32339.
Long NM, Kuhl BA (2021) Cortical representations of visual stimuli shift locations with changes in memory states. Curr Biol 31:1119–1126.e5.
Long B, Yu C-P, Konkle T (2018) Mid-level visual features underlie the high-level categorical organization of the ventral stream. Proc Natl Acad Sci U S A 115:E9015–E9024.
Lundstrom BN, Ingvar M, Petersson KM (2005) The role of precuneus and left inferior frontal cortex during source memory episodic retrieval. Neuroimage 27:824–834.
Maldjian JA, Laurienti PJ, Burdette JH (2004) Precentral gyrus discrepancy in electronic versions of the Talairach atlas. Neuroimage 21:450–455.
Maldjian JA, Laurienti PJ, Kraft RA, Burdette JH (2003) An automated method for neuroanatomic and cytoarchitectonic atlas-based interrogation of fMRI data sets. Neuroimage 19:1233–1239.
Maris E, Oostenveld R (2007) Nonparametric statistical testing of EEG- and MEG-data. J Neurosci Methods 164:177–190.
Marr D (1971) Simple memory: a theory for archicortex. Philos Trans R Soc Lond B Biol Sci 262:23–81.
Martin CB, Douglas D, Newsome RN, Man LL, Barense MD (2018) Integrative and distinctive coding of visual and conceptual object features in the ventral visual stream. Elife 7:e31873.
McClelland JL, McNaughton BL, O'Reilly RC (1995) Why there are complementary learning systems in the hippocampus and neocortex: insights from the successes and failures of connectionist models of learning and memory. Psychol Rev 102:419–457.
Michelmann S, Staresina BP, Bowman H, Hanslmayr S (2019) Speed of time-compressed forward replay flexibly changes in human episodic memory. Nat Hum Behav 3:143–154.
Mirjalili S, Powell P, Strunk J, James T, Duarte A (2021) Context memory encoding and retrieval temporal dynamics are modulated by attention across the adult lifespan. eNeuro 8: ENEURO.0387-20.2020.
Misaki M, Kim Y, Bandettini PA, Kriegeskorte N (2010) Comparison of multivariate classifiers and response normalizations for pattern-information fMRI. Neuroimage 53:103–118.
Moscovitch M (2008) The hippocampus as a 'stupid,' domain-specific module: implications for theories of recent and remote memory, and of imagination. Can J Exp Psychol 62:62–79.
Naghavi HR, Nyberg L (2005) Common fronto-parietal activity in attention, memory, and consciousness: shared demands on integration? Conscious Cogn 14:390–425.
Nichols TE, Holmes AP (2002) Nonparametric permutation tests for functional neuroimaging: a primer with examples. Hum Brain Mapp 15:1–25.
Nili H, Wingfield C, Walther A, Su L, Marslen-Wilson W, Kriegeskorte N (2014) A toolbox for representational similarity analysis. PLoS Comput Biol 10:e1003553.
Noppeney U, Price CJ (2002) A PET study of stimulus- and task-induced semantic processing. Neuroimage 15:927–935.
Oostenveld R, Fries P, Maris E, Schoffelen J-M (2010) Fieldtrip: open source software for advanced analysis of MEG, EEG, and invasive electrophysiological data. Comput Intell Neurosci 2011:e156869.
O'Reilly RC, McClelland JL (1994) Hippocampal conjunctive encoding, storage, and recall: avoiding a trade-off. Hippocampus 4:661–682.
O'Reilly RC, Norman KA (2002) Hippocampal and neocortical contributions to memory: advances in the complementary learning systems framework. Trends Cogn Sci 6:505–510.
Patterson K, Nestor PJ, Rogers TT (2007) Where do you know what you know? The representation of semantic knowledge in the human brain. Nat Rev Neurosci 8:976–987.
Pelli DG (1997) The VideoToolbox software for visual psychophysics: transforming numbers into movies. Spat Vis 10:437–442.
Penny W, Friston K, Ashburner J, Kiebel S, Nichols T (2007) *Statistical parametric mapping: the analysis of functional brain images*. London: Academic Press/Elsevier.
Polyn SM, Natu VS, Cohen JD, Norman KA (2005) Category-specific cortical activity precedes retrieval during memory search. Science 310:1963–1966.
Poser BA, Versluis MJ, Hoogduin JM, Norris DG (2006) BOLD contrast sensitivity enhancement and artifact reduction with multiecho EPI: parallel-acquired inhomogeneity-desensitized fMRI. Magn Reson Med 55:1227–1235.
Quiroga RQ (2012) Concept cells: the building blocks of declarative memory functions. Nat Rev Neurosci 13:587–597.
Rice GE, Caswell H, Moore P, Hoffman P, Lambon Ralph MA (2018) The roles of left versus right anterior temporal lobes in semantic memory: a neuropsychological comparison of postsurgical temporal lobe epilepsy patients. Cereb Cortex 28:1487–1501.
Rissman J, Wagner AD (2012) Distributed representations in memory: insights from functional brain imaging. Annu Rev Psychol 63:101–128.
Ritchey M, Cooper RA (2020) Deconstructing the posterior medial episodic network. Trends Cogn Sci 24:451–465.
Ritchey M, Wing EA, LaBar KS, Cabeza R (2013) Neural similarity between encoding and retrieval is related to memory via hippocampal interactions. Cereb Cortex 23:2818–2828.
Rolls ET (2010) A computational theory of episodic memory formation in the hippocampus. Behav Brain Res 215:180–196.
Rolls ET (2013) The mechanisms for pattern completion and pattern separation in the hippocampus. Front Syst Neurosci 7:74.
Rorden C, Brett M (2000) Stereotaxic display of brain lesions. Behav Neurol 12:191–200.
RSA Group (2019) RSA toolbox [Computer software]. Available at: https://github.com/rsagroup/rsatoolbox
Schyns PG, Zhan J, Jack RE, Ince RAA (2020) Revealing the information contents of memory within the stimulus information representation framework. Philos Trans R Soc Lond B Biol Sci 375:20190705.
Shen J (2014) Tools for NIfTI and ANALYZE image (version 1.27.0.0) [Computer software]. MATLAB Central File Exchange. Available at: https://uk.mathworks.com/matlabcentral/fileexchange/8797-tools-for-nifti-and-analyze-image (Retrieved December 8, 2017)
Simons JS, Ritchey M, Fernyhough C (2022) Brain mechanisms underlying the subjective experience of remembering. Annu Rev Psychol 73:159–186.
Smith SM, Nichols TE (2009) Threshold-free cluster enhancement: addressing problems of smoothing, threshold dependence and localisation in cluster inference. Neuroimage 44:83–98.
St-Laurent M, Abdi H, Buchsbaum BR (2015) Distributed patterns of reactivation predict vividness of recollection. J Cogn Neurosci 27:2000–2018.
Staresina BP, Henson RNA, Kriegeskorte N, Alink A (2012) Episodic reinstatement in the medial temporal lobe. J Neurosci 32:18150–18156.
Staresina BP, Wimber M (2019) A neural chronometry of memory recall. Trends Cogn Sci 23:1071–1085.
Teyler TJ, DiScenna P (1986) The hippocampal memory indexing theory. Behav Neurosci 100:147–154.
Teyler TJ, Rudy JW (2007) The hippocampal indexing theory and episodic memory: updating the index. Hippocampus 17:1158–1169.

Thakral PP, Wang TH, Rugg MD (2015) Cortical reinstatement and the confidence and accuracy of source memory. Neuroimage 109:118–129.
The GIMP Development Team (2019) GIMP [Computer software]. Available at: https://www.gimp.org
The MathWorks Inc. (2014) MATLAB (Version 8.4 (R2014b)) [Computer software]. Available at: https://www.mathworks.com
The MathWorks Inc. (2016) MATLAB (Version 9.0 (R2016a)) [Computer software]. Available at: https://www.mathworks.com
The MathWorks Inc. (2017) MATLAB (Version 9.3 (R2017b)) [Computer software]. Available at: https://www.mathworks.com
Thornton MA, Ince R, Charest I (2016) MatlabTFCE [Computer software]. Available at: https://github.com/markallenthornton/MatlabTFCE/tree/master
Treder MS (2020) MVPA-light: a classification and regression toolbox for multi-dimensional data. Front Neurosci 14:289.
Tulving E, Le Voi ME, Routh DA, Loftus E, Broadbent DE (1983) Ecphoric processes in episodic memory. Philos Trans R Soc Lond B Biol Sci 302:361–371.
Tzourio-Mazoyer N, Landeau B, Papathanassiou D, Crivello F, Etard O, Delcroix N, Mazoyer B, Joliot M (2002) Automated anatomical labeling of activations in SPM using a macroscopic anatomical parcellation of the MNI MRI single-subject brain. Neuroimage 15:273–289.
van Rossum G (1995) Python tutorial. Centrum Wiskunde & Informatica. Available at: https://ir.cwi.nl/pub/5007
Vidaurre D, Cichy RM, Woolrich MW (2021) Dissociable components of information encoding in human perception. Cereb Cortex 31:5664–5675.
Virtanen P, Gommers R, Oliphant TE, Haberland M, Reddy T, Cournapeau D, Burovski E, Peterson P, Weckesser W, Bright J (2020a) SciPy 1.0: fundamental algorithms for scientific computing in Python. Nat Methods 17:261–533.
Virtanen P, Gommers R, Oliphant TE, Haberland M, Reddy T, Cournapeau D, Burovski E, Peterson P, Weckesser W, Bright J (2020b) Author Correction: SciPy 1.0: fundamental algorithms for scientific computing in Python. Nat Methods 17:352.
Visser M, Jefferies E, Lambon Ralph MA (2010) Semantic processing in the anterior temporal lobes: a meta-analysis of the functional neuroimaging literature. J Cogn Neurosci 22:1083–1094.
Wagner AD, Shannon BJ, Kahn I, Buckner RL (2005) Parietal lobe contributions to episodic memory retrieval. Trends Cogn Sci 9:445–453.
Weaverdyck ME, Lieberman MD, Parkinson C (2020) Tools of the trade multivoxel pattern analysis in fMRI: a practical introduction for social and affective neuroscientists. Soc Cogn Affect Neurosci 15:487–509.
Wheeler ME, Petersen SE, Buckner RL (2000) Memory's echo: vivid remembering reactivates sensory-specific cortex. Proc Natl Acad Sci U S A 97:11125–11129.
Wing EA, Ritchey M, Cabeza R (2014) Reinstatement of individual past events revealed by the similarity of distributed activation patterns during encoding and retrieval. J Cogn Neurosci 27:679–691.
Xiao X, Dong Q, Gao J, Men W, Poldrack RA, Xue G (2017) Transformed neural pattern reinstatement during episodic memory retrieval. J Neurosci 37:2986–2998.
Xie S, Kaiser D, Cichy RM (2020) Visual imagery and perception share neural representations in the alpha frequency band. Curr Biol 30:2621–2627.e5.
Xue G (2022) From remembering to reconstruction: the transformative neural representation of episodic memory. Prog Neurobiol 219:102351.